Check for updates

New Phytologist

Seasonal trends in leaf-level photosynthetic capacity and water use efficiency in a North American Eastern deciduous forest and their impact on canopy-scale gas exchange

Kenneth J. Davidson[1,2], Julien Lamour[1], Anna McPherran[2], Alistair Rogers[1] and Shawn P. Serbin[1,2]

[1]Department of Environmental and Climate Sciences, Brookhaven National Laboratory, Upton, NY 11973, USA; [2]Department of Ecology and Evolution, Stony Brook University, Stony Brook, NY 11794, USA

Author for correspondence:
Kenneth J. Davidson
Email: kdavidson.sci@gmail.com

Received: *16 December 2022*
Accepted: *24 June 2023*

New Phytologist (2023) **240:** 138–156
doi: 10.1111/nph.19137

Key words: earth system models, g_1, gas exchange, phenology, seasonal physiology, V_{cmax}, water use efficiency.

Summary

- Vegetative transpiration (E) and photosynthetic carbon assimilation (A) are known to be seasonally dynamic, with changes in their ratio determining the marginal water use efficiency (WUE). Despite an understanding that stomata play a mechanistic role in regulating WUE, it is still unclear how stomatal and nonstomatal processes influence change in WUE over the course of the growing season. As a result, limited understanding of the primary physiological drivers of seasonal dynamics of canopy WUE remains one of the largest uncertainties in earth system model projections of carbon and water exchange in temperate deciduous forest ecosystems.
- We investigated seasonal patterns in leaf-level physiological, hydraulic, and anatomical properties, including the seasonal progress of the stomatal slope parameter (g_1; inversely proportional to WUE) and the maximum carboxylation rate (V_{cmax}).
- V_{cmax} and g_1 were seasonally variable; however, their patterns were not temporally synchronized. g_1 generally showed an increasing trend until late in the season, while V_{cmax} peaked during the midsummer months. Seasonal progression of V_{cmax} was primarily driven by changes in leaf structural, and anatomical characteristics, while seasonal changes in g_1 were most strongly related to changes in V_{cmax} and leaf hydraulics.
- Using a seasonally variable V_{cmax} and g_1 to parameterize a canopy-scale gas exchange model increased seasonally aggregated A and E by 3% and 16%, respectively.

Introduction

Vegetation regulates the exchanges of water vapor to the atmosphere via transpiration (E) and the uptake of carbon from the atmosphere via photosynthetic carbon assimilation (A); thus, models which aim to predict carbon and water balance across space and through time must account for the temporal and spatial variation in E and A (Blyth *et al.*, 2021). Accounting for the seasonal variability associated with these processes is a major challenge for earth system models (ESMs), which often employ trait-based proxies to represent seasonal progression in potential for transpiration and assimilation (Rogers *et al.*, 2017). However, these proxies may not fully capture the mechanisms underpinning the drivers of seasonal variation in E and A, nor do they accurately address how variation in E and A may co-vary over the course of a growing season. This critical knowledge gap hampers the predictive accuracy of ESMs and has been identified as an area for model improvement (Jefferson *et al.*, 2017).

Earth system models represent E and A using a system of equations (e.g. Farquhar *et al.*, 1980) that link photosynthetic carbon gain (von Caemmerer & Farquhar, 1981) to water loss via stomata (Ball *et al.*, 1987; Medlyn *et al.*, 2011). The marginal variation of A and E, known as the water use efficiency ($\partial A/\partial E$, WUE), is represented in the unified stomatal optimization model (Medlyn *et al.*, 2011) as the inverse of the stomatal slope parameter (g_1, $kPa^{0.5}$). Thus, the relationship between A and stomatal conductance (g_{sw}) for a given set of environmental conditions is dictated by g_1, combined with the value of the stomatal intercept (g_0, mol m^{-2} s^{-1}, the expected g_{sw} when net assimilation (A_{net}) is zero). Among the parameters necessary to estimate A (Bernacchi *et al.*, 2013) are the maximum carboxylation rate of the enzyme Rubisco (V_{cmax}, μmol m^{-2} s^{-1}) and the rate of respiratory CO_2 release in the dark (R_{dark}, μmol m^{-2} s^{-1}). While accurate estimation of stomatal and photosynthetic parameters is essential to properly represent the role of vegetation in regulating net primary productivity (NPP) and transpiration across space and time, a general lack of paired foliar trait and physiology data (e.g. Wright *et al.*, 2004; Kattge *et al.*, 2011) across diverse plant functional types (PFTs) still hampers modeling efforts (Reich *et al.*, 2007). In particular, lack of process-based knowledge for representing PFT-specific parametrization of stomatal traits remains one of the largest uncertainties in current model predictions of the functioning of North American forests (Dietze *et al.*, 2014; Jefferson *et al.*, 2017; Ricciuto *et al.*, 2018).

© 2023 The Authors.
New Phytologist © 2023 New Phytologist Foundation
This article has been contributed to by U.S. Government employees and their work is in the public domain in the USA.

14698137, 2023, 1, Downloaded from https://nph.onlinelibrary.wiley.com/doi/10.1111/nph.19137 by Columbia University Libraries, Wiley Online Library on [05/09/2024]. See the Terms and Conditions (https://onlinelibrary.wiley.com/terms-and-conditions) on Wiley Online Library for rules of use; OA articles are governed by the applicable Creative Commons License

Table 1 Average species-group-specific values for photosynthetic and conductance parameters used in fixed model simulations of canopy *E* and NPP, and approximate date of leaf out and leaf coloration.

Group	Species	Sample size	$V_{cmax.25}$ (μmol m^{-2} s^{-1})	$R_{dark.25}$ (μmol m^{-2} s^{-1})	g_1 (kPa$^{0.5}$)	g_0 (mol m^{-2} s^{-1})	Leaf out (DOY)	Leaf coloration (DOY)
Birch	*Betula alleghaniensis* Britt.	69	35.92^{A} (1.9)	1.06^{A} (0.05)	2.47^{A} (0.13)	0.033^{A} (0.0046)	131	257
Maple	*Acer rubrum* L. *Acer saccharum* Marshall	68	32.91^{A} (1.59)	0.96^{A} (0.05)	1.45^{B} (0.08)	0.011^{B} (0.0017)	126	263
White oak	*Quercus alba* L. *Quercus montana* Willd.	66	28.09^{A} (2.42)	1.34^{B} (0.07)	0.91^{C} (0.12)	0.012^{B} (0.0026)	139	286
Red oak	*Quercus rubra* L.	69	39.74^{A} (2.41)	1.34^{B} (0.08)	1.95^{A} (0.14)	0.013^{B} (0.0029)	124	273

Each sample represents an independent leaf-level estimate. Values in parentheses are the SE of the species-group mean estimate. Superscript letters indicate significant ($P < 0.05$) pairwise differences between parameter estimates obtained from *post hoc* Tukey tests.

Accounting for seasonal variability associated with photosynthetic and stomatal parameters is an additional challenge when parameterizing models (Wilson *et al.*, 2000a, 2001; Xu & Baldocchi, 2003; Grassi *et al.*, 2005; Wang *et al.*, 2008; Ow *et al.*, 2010; Stokes *et al.*, 2010; Bauerle *et al.*, 2012; Ali *et al.*, 2015; Way & Montgomery, 2015; Chu *et al.*, 2018; Burnett *et al.*, 2021). Given the lack of seasonal data, some modeling efforts use trait-based proxies to represent seasonal change in photosynthetic capacity (Rogers *et al.*, 2017) such as seasonal trends in foliar nitrogen content or leaf mass per area (LMA) as a proxy for seasonal trends in V_{cmax} (Ellsworth & Reich, 1993; Medlyn *et al.*, 1999; Meir *et al.*, 2002; Misson *et al.*, 2006). These models, which use the principle of optimal allocation of nitrogen such that photosynthetic potential is maximized (Quebbeman & Ramirez, 2016), have recently been shown to be capable of explaining up to 83% of seasonal variation in V_{cmax} globally (Jiang *et al.*, 2020). However, trait-based relationships are known to vary considerably by PFT (Kattge *et al.*, 2009), or by the fraction of nitrogen allocated to Rubisco (Luo *et al.*, 2021). Other models prescribe a value for V_{cmax}, which can be modified seasonally in conjunction with bioclimatic factors such as growth temperature (Medvigy *et al.*, 2009), photoperiod (Bauerle *et al.*, 2012), or soil moisture (Wang *et al.*, 2022). In some cases (Ali *et al.*, 2015; Smith *et al.*, 2019), this latter method has been shown to be superior to trait-based approaches.

While there has been considerable effort dedicated to assessing mechanisms of seasonal variation in V_{cmax}, we know much less about the seasonal or ontogenetic patterns of leaf WUE, where the effects of season, drought, and phenology are often interrelated. Past work has mostly focused on drought effects (Sala & Tenhunen, 1996; Xu & Baldocchi, 2003; Grassi & Magnani, 2005; Héroult *et al.*, 2013; Sperlich *et al.*, 2016; Xie *et al.*, 2016), finding that seasonal increases in WUE are associated with progressive drought stress. In studies without a pronounced seasonal drought effect (Zhu *et al.*, 2011; Sanchez *et al.*, 2013; Miao *et al.*, 2021), WUE has been observed to decrease as leaves approached senescence, with a late season peak in stomatal slope. Furthermore, models of foliar transpiration which account for leaf ontogeny suggest that cuticular leakage and incomplete stomatal closure contribute to elevated g_0 at the start and end of the growth season (Gee & Federer, 1972; Wardle & Short, 1983; Kane *et al.*, 2020). Recently, Jin *et al.* (2022) demonstrated that phenology of leaf area index (LAI) can be used to improve seasonal characterization of canopy g_1 which led to improved predictions of seasonal *E*. Additional work has linked stomatal traits with seasonal climatic conditions, such as growth season temperature (Jin *et al.*, 2017) or photoperiod (Bauerle *et al.*, 2012). Evidence also suggests that moisture availability and atmospheric humidity may partially regulate WUE seasonality, explaining up to 35% of the global variation in g_1 (Lin *et al.*, 2015).

Despite some remaining uncertainties surrounding the seasonality of leaf physiology, variation in photosynthetic capacity associated with a seasonal scalar has been incorporated into a number of common ESMs (Krinner *et al.*, 2005; Medvigy *et al.*, 2009; Oleson *et al.*, 2013) and optimality schemes (Sabot *et al.*, 2022; Prikaziuk *et al.*, 2023) via a seasonal modification of the V_{cmax} parameter. Debate still remains, however, regarding the correct function used to represent this seasonal change (Medvigy *et al.*, 2013; Chen *et al.*, 2021; Mengoli *et al.*, 2022). Modification of V_{cmax} affects both rates of A and g_{sw} and thus has the potential to indirectly alter WUE. However, aside from models which temporarily reduce g_0, g_1, or both in response to a soil moisture stress β-factor (De Kauwe *et al.*, 2013; Rogers *et al.*, 2017; Li *et al.*, 2022), no ESMs, to our knowledge, directly alter WUE through a modification of stomatal parameters associated with leaf ontogeny or environmental conditions.

In this study, we measured the seasonal patterns of a suite of foliar parameters related to WUE (g_1 and g_0) and photosynthetic capacity scaled from measurement temperature to 25°C ($V_{cmax.25}$, and $R_{dark.25}$) in four tree species groups (Table 1) that are common to the Northeastern United States and have high economic and ecological value. We collected data on foliar physiology and leaf traits every 3 wk for the full 2021 growth season and used these data in a canopy-scale gas exchange model like the one used in an ESM. We address four key research questions: (1) What are the seasonal patterns in foliar WUE and photosynthetic parameters? (2) What are the biotic and abiotic controls of foliar physiological trait development, and how do they relate to the anatomical, structural, and hydraulic changes associated with leaf ontogeny?

© 2023 The Authors.
New Phytologist © 2023 New Phytologist Foundation
This article has been contributed to by U.S. Government employees and their work is in the public domain in the USA.

(3) Does ontogeny modify the assumed linear relationships between photosynthetic parameters and leaf traits, and can these linear relationships be extended to stomatal parameters as well? (4) How does a model parameterization which explicitly considers seasonal dynamics of WUE and photosynthetic capacity impact the modeling of transpiration (E) and canopy carbon assimilation (A) compared with a model parameterization which holds WUE and photosynthetic capacity constant at the seasonal mean value?

Materials and Methods

Study site and species

All data were collected at the Black Rock Forest (BRF), a 1550 ha protected, secondary growth forest located in the Hudson Highlands Region of New York (Fig. 1a). The site has a humid, subtropical climate, receiving an average of 1.2 m of precipitation per growth season, and with a mean growth season temperature of 23.4°C (Turnbull *et al.*, 2001; Schuster *et al.*, 2008; Fig. 2). We collected data from three sites within the forest, each with similar soil and species composition (Fig. 1a). The forest is dominated by deciduous species, with a composition of *c.* 67% oaks, *c.* 31% nonoak deciduous hardwoods, and *c.* 2% conifers (Schuster *et al.*, 2008; Falxa-Raymond *et al.*, 2012), with a mean LAI of $4.59 \pm 0.12\ m^2\ m^{-2}$, measured in July using an LAI-2200 (Li-Cor Inc., Lincoln, NE, USA). Roughly every 3 wk between 17 May and 15 October 2021, we collected data on six deciduous hardwood species, which we aggregated into four groups (hereafter 'groups') based on functional type (see Table 1 for details). During each sample collection, we targeted the most fully expanded and physiologically mature leaf on each sampled branch with the aim of measuring the same cohort of leaves over the course of a growing season.

Branches were collected via shotgun sampling (Serbin *et al.*, 2014; Burnett *et al.*, 2021), using a 12-gauge shotgun and steel bird shot (Fig. 1b). All branch sampling occurred between nautical twilight and sunrise. Once branches fell, they were immediately recut under water to prevent cavitation or embolism of the xylem. After an initial 20 cm cut was made, multiple smaller cuts (5–15 cm) were made to progressively ease xylem tension (Sperry, 2013). After processing, all branch segments measured between 100 and 200 cm.

Gas exchange

Gas exchange measurements were conducted in the laboratory using three LI-6800 and two LI-6400XT portable photosynthesis systems (Li-Cor Inc.). For all measurements, the color spectrum of the irradiance was the same (90% red, 10% blue). We conducted stomatal response curves to estimate stomatal and photosynthetic parameters (Ball *et al.*, 1987; Leakey *et al.*, 2006; Davidson *et al.*, 2022). With this method, irradiance is adjusted to propagate changes in A, while maintaining a constant level of sample CO_2 concentration (CO_2S) and VPD_{leaf} within each response curve (Fig. 1c). Using previously published data on the response of A to irradiance for our study species (Dreyer *et al.*, 2001), we estimated the full range of irradiance, ranging from light-saturated photosynthesis (A_{sat}), to respiratory CO_2 release in the dark (R_{dark}). All measurements were made at a leaf temperature of 24–27°C and with VPD_{leaf} between 0.8 and 1.4 kPa. On average, T_{leaf} was 26.25°C and VPD_{leaf} was 1.07 kPa. Data were automatically logged every 10 s for the duration of measurements. After a 1-h acclimation and stabilization period at the first irradiance level, light was reduced to the next lowest irradiance level, and leaves were allowed to acclimate to this new irradiance level for a minimum of 20 min until rates of A and g_{sw} reached a steady state. This process was repeated until measurements at all 11 irradiance levels had been completed. For each irradiance level, an average of the 5 log points before a change in irradiance represented each measurement point.

After gas exchange measurements were taken, we used a cork borer to obtain leaf disks of a known area and measured leaf disk fresh mass. These disks were then dried to a constant mass in a 60°C oven and weighed to obtain dry mass. We then estimated LMA (dry mass/leaf area) and leaf dry matter content (LDMC; dry mass/fresh mass). Finally, a subset of the dried leaf samples were ground, and elemental nitrogen and carbon was quantified using a 2400 Series II CHN analyzer (PerkinElmer, Waltham, MA, USA) to estimate nitrogen as expressed on an area and mass basis (N_{area}, N_{mass}).

Leaf hydraulics

In addition to gas exchange, we measured a suite of leaf-level hydraulic properties on all collected branches to determine how changes in leaf hydraulics related to other physiological changes associated with leaf ontogeny. Once each branch was collected, a leaf was immediately removed at the base of the petiole and sealed in an airtight, humid, cool, dark box for transport to the laboratory. Leaf water potential (Ψ_{leaf}) was measured with a Scholander-type pressure chamber (Scholander *et al.*, 1964). This measurement of predawn Ψ_{leaf} served as a quantitative assessment of branch hydraulic stress and enabled prescreening of branches before other measurements (Rodriguez-Dominguez *et al.*, 2022).

We also performed pressure–volume (PV) curves on one leaf from each branch following the method of Bartlett *et al.* (2012). Branches were rehydrated for a period of 1.5 h before analysis. Using a razor, leaf samples were removed from the rehydrated branches and Ψ_{leaf} and sample mass were recorded. Samples were then allowed to dry for 10 h, with Ψ_{leaf} and sample mass recorded 8–12 times during this period. After this, samples were dried to constant mass in a 60°C oven, and a dry mass value was recorded. We assessed the relationship between the water potential and relative water content using the R package PVLDCURVE (v.1.2.6; Raesch, 2020) to determine the turgor loss point (Ψ_{TLP}), relative water deficit at the turgor loss point (RWD_{TLP}, %), and the bulk elastic modulus (ε).

Stomatal anatomy

Using a thin layer of clear coat nail varnish, we obtained impressions of the abaxial side of two leaves per branch sample. Images of these impressions were captured using a stage microscope with a digital camera attachment (Nikon ECLIPSE Ci/Ni, Tokyo,

© 2023 The Authors.
New Phytologist © 2023 New Phytologist Foundation
This article has been contributed to by U.S. Government employees and their work is in the public domain in the USA.

14698137, 2023, 1, Downloaded from https://nph.onlinelibrary.wiley.com/doi/10.1111/nph.19137 by Columbia University Libraries, Wiley Online Library on [05/09/2024]. See the Terms and Conditions (https://onlinelibrary.wiley.com/terms-and-conditions) on Wiley Online Library for rules of use; OA articles are governed by the applicable Creative Commons License

14698137, 2023, 1, Downloaded from https://nph.onlinelibrary.wiley.com/doi/10.1111/nph.19137 by Columbia University Libraries, Wiley Online Library on [05/09/2024]. See the Terms and Conditions (https://onlinelibrary.wiley.com/terms-and-conditions) on Wiley Online Library for rules of use; OA articles are governed by the applicable Creative Commons License

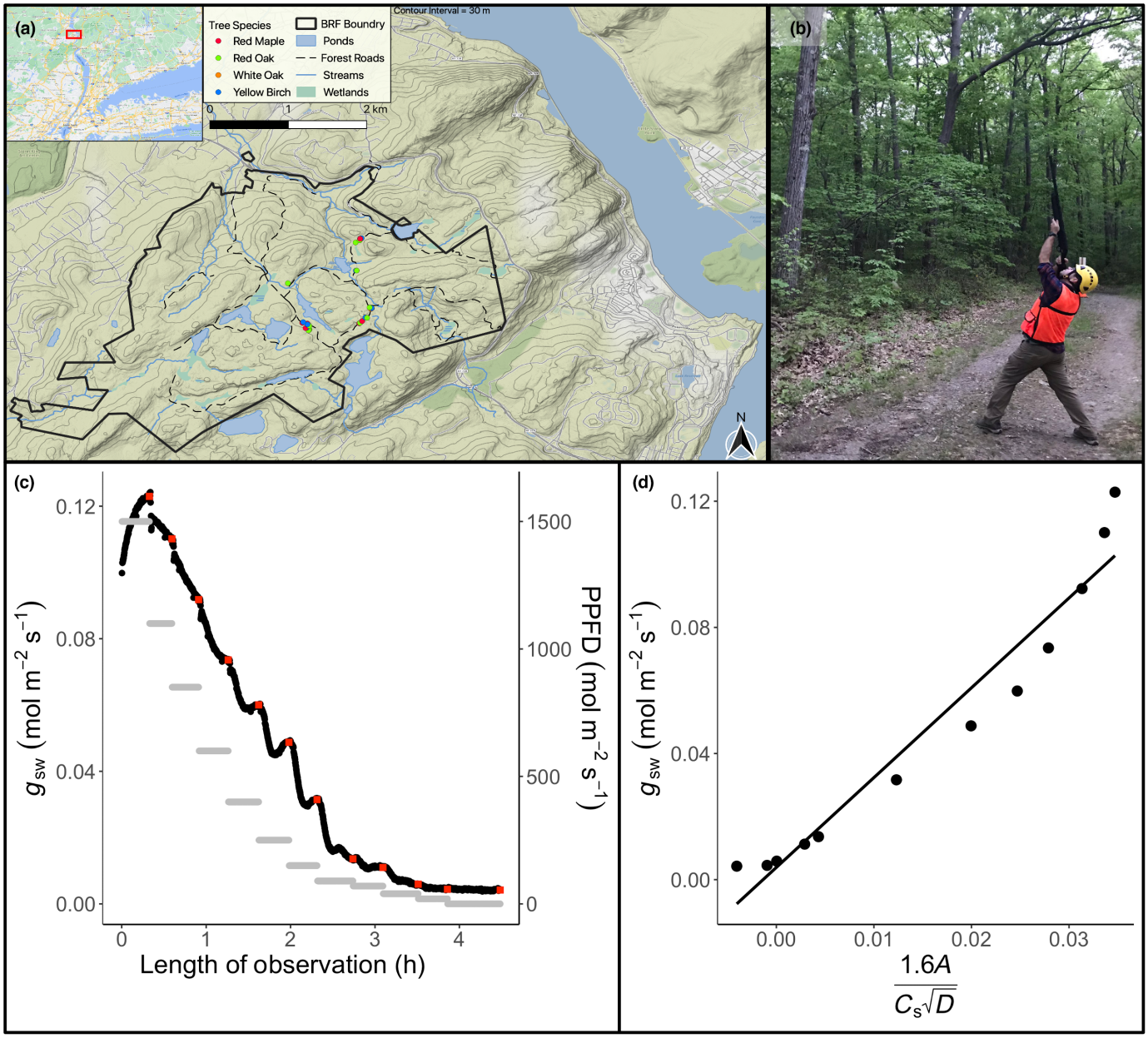


Fig. 1 Schematic representation of sampling method and estimation of stomatal response parameters. (a) Geographic location of Black Rock Forest (41.45°N, 74.01°W, 110–450 m above sea level), and distribution of study trees at the site; (b) using a 12-gauge shotgun to sample upper canopy vegetation; (c) raw data from the response of stomatal conductance (g_{sw}) to decreasing irradiance, with black points representing individual observations of g_{sw}, red points representing the final extracted rates of g_{sw}, and horizontal gray bars representing irradiance levels (1500, 900, 700, 450, 250, 175, 90, 40, 20, and 0 μmol m^{-2} s^{-1}); (d) regression fit of the g_{sw} values extracted from the curve in (c) vs the leaf-level environmental conditions at the time of measurement. C_s and D are the leaf surface CO_2 concentration and vapor pressure deficit, respectively, and A is the net photosynthetic rate.

Japan) at ×400 magnification. Using these images, we estimated stomatal density (number of stomata per mm^2) and stomatal area (length × width of the guard cells), averaging these measurements by group for each month.

Estimation of gas exchange parameters

The stomatal parameters g_1 and g_0 were estimated using the unified stomatal optimization model (USO, Medlyn *et al.*, 2011, Eqn 1).

$$g_s = g_0 + 1.6\left(1 + \frac{g_1}{\sqrt{\mathrm{VPD}_{leaf}}}\right)\frac{A}{C_s} \quad \text{Eqn 1}$$

where g_0 represents the expected g_{sw} when $A_n = 0$, C_s and VPD_{leaf} are the leaf surface CO_2 concentration and vapor pressure deficit, respectively, and g_1 is a slope parameter inversely proportional to WUE ($\partial E/\partial A$).

We estimated V_{cmax} for each leaf using the 'one-point method' (De Kauwe *et al.*, 2016, Eqn 2), where we allowed time for full

© 2023 The Authors.
New Phytologist © 2023 New Phytologist Foundation
This article has been contributed to by U.S. Government employees and their work is in the public domain in the USA.

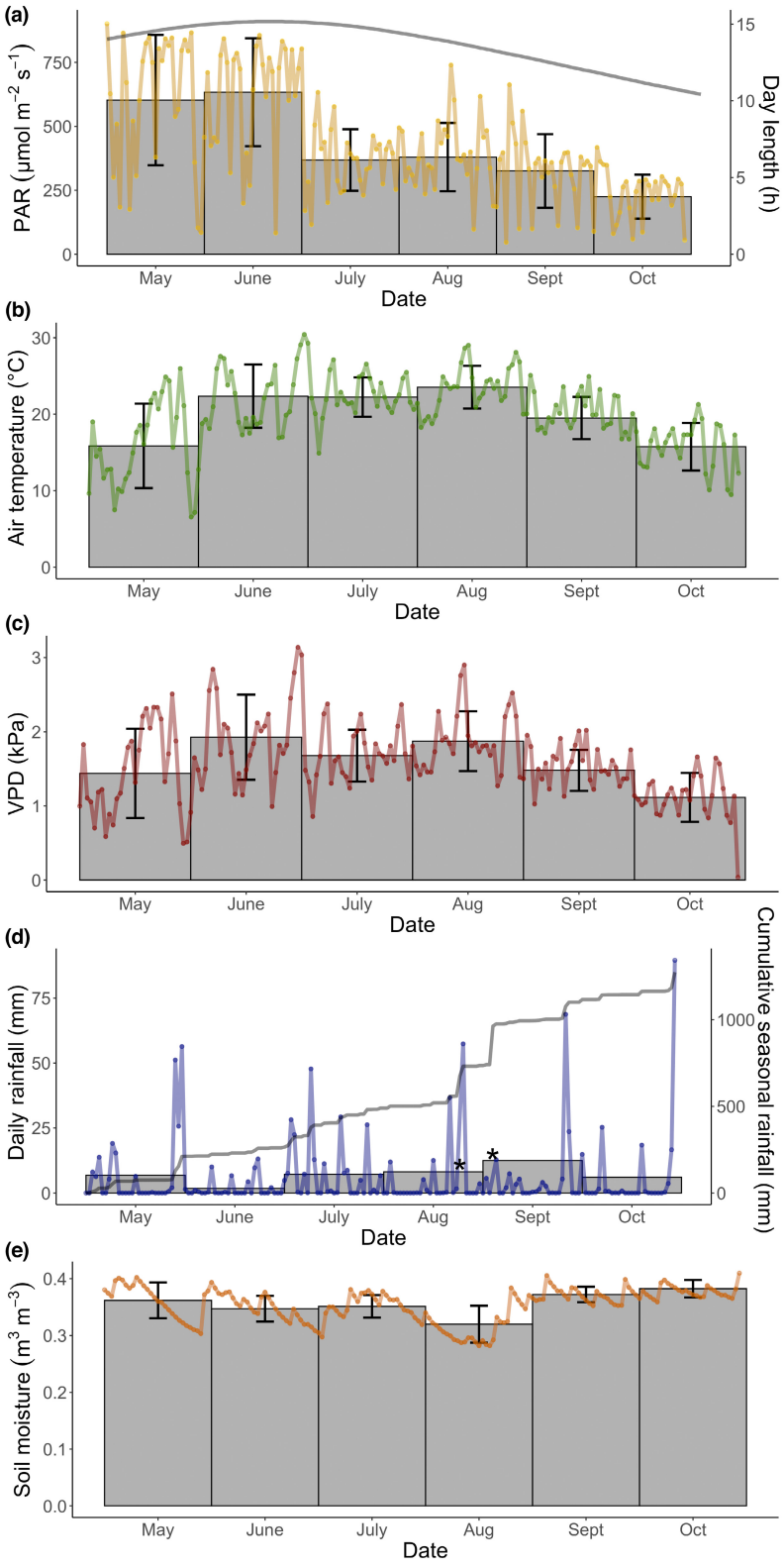


Fig. 2 Meteorological conditions at Black Rock Forest for the 2021 growth season. Data in (a–d) are an average from two meteorological stations within the forest, each recording hourly average measurements, while data in (e) come from the ERA5-Land reanalysis dataset (Muñoz Sabater, 2019). Daytime is defined as the interval from local sunrise to sunset. During the period of study, mean daily temperature was 19.7°C and total precipitation was 1.1 m (a) mean daytime irradiance (photosynthetically active radiation) and day length, (b) mean daytime air temperature, (c) mean daytime vapor pressure deficit (VPD), (d) total daily (24-h) and cumulative seasonal rainfall, and (e) mean daily (24-h) volumetric soil moisture content. For all plots, individual points are single-day observations, and gray bars are monthly average with error bars representing ±2 SE of the mean. Asterisks in (d) are abnormal rainfall events (not plotted), 22 August (125 mm) and 1 September (222 mm).

© 2023 The Authors.
New Phytologist © 2023 New Phytologist Foundation
This article has been contributed to by U.S. Government employees and their work is in the public domain in the USA.

14698137, 2023, 1, Downloaded from https://nph.onlinelibrary.wiley.com/doi/10.1111/nph.19137 by Columbia University Libraries, Wiley Online Library on [05/09/2024]. See the Terms and Conditions (https://onlinelibrary.wiley.com/terms-and-conditions) on Wiley Online Library for rules of use; OA articles are governed by the applicable Creative Commons License

14698137, 2023, 1, Downloaded from https://nph.onlinelibrary.wiley.com/doi/10.1111/nph.19137 by Columbia University Libraries, Wiley Online Library on [05/09/2024]. See the Terms and Conditions (https://onlinelibrary.wiley.com/terms-and-conditions) on Wiley Online Library for rules of use; OA articles are governed by the applicable Creative Commons License

acclimation to the light environment. This approach has shown comparable results to traditional AC_i curves in other eastern deciduous species (Burnett *et al.*, 2019):

$$V_{cmax} = \frac{A_{sat}}{\left(\frac{C_i - \Gamma^*}{C_i + K_m} - 0.015\right)} \quad \text{Eqn 2}$$

where K_m is the Michaelis–Menten constant (404.9 μmol mol^{-1}; Supporting Information Table S1; Bernacchi *et al.*, 2001), Γ* is the CO_2 compensation point in the absence of mitochondrial respiration (42.75 μmol mol^{-1}; Table S1; Bernacchi *et al.*, 2001), and C_i is the intercellular CO_2 concentration.

We used the initial acclimated, steady-state, light-saturated point of each stomatal response curve for our measurement of A_{sat} and its corresponding C_i. To scale V_{cmax} at measurement temperature to V_{cmax} at 25°C ($V_{cmax.25}$), we used a modified Arrhenius equation (Leuning, 2002, Eqn 3) with kinetic constants specific to each group (Table S1; Dreyer *et al.*, 2001):

$$V_{cmax.25} = \frac{V_{cmax.T}}{C \times \exp\left[\left(\frac{H_a}{RT_{25}}\right) \times \left(\frac{1 - T_{25}}{T_{leaf}}\right)\right] \times 1 + \exp\left[\frac{(S_V T_{leaf} - H_d)}{RT_{leaf}}\right]} \quad \text{Eqn 3}$$

where $V_{cmax.25}$ is the value of V_{cmax} at the reference temperature ($T_{25} = 298.15$ K), $V_{cmax.T}$ is the value of V_{cmax} at the leaf temperature (T_{leaf} in K), H_a, H_d, and S_v are the activation and deactivation energies of the enzyme Rubisco and an entropy term (J mol^{-1}; J mol^{-1}; J mol^{-1} K^{-1}), R is the ideal gas constant ($R = 8.314$ J mol^{-1} K^{-1}), and C is a combined term equivalent to $1 + \exp[(S_v T_{25} - H_d)/(RT_{25})]$.

Finally, R_{dark} was calculated from dark-adapted measurements of A (the final stomatal response curve point) and was scaled to 25°C ($R_{dark.25}$) using an inverse Arrhenius equation (Eqn 4; Bernacchi *et al.*, 2001; Von Caemmerer, 2013):

$$R_{dark.25} = \frac{R_{dark}}{\exp\left(\frac{H_a}{(R \times T_{25})} - \frac{H_a}{(R \times T_{leaf})}\right)} \quad \text{Eqn 4}$$

where H_a is the group-specific activation energy of mitochondrial respiration (Table S1; J mol^{-1}).

Canopy assimilation and transpiration simulations

To assess how seasonality in photosynthetic and stomatal parameters may impact simulated rates of canopy E and A, we used the function 'f.GPPT' included in the R package LEAFGASEXCHANGE (v.1.0.1; Lamour & Serbin, 2021) which combines a coupled leaf-scale steady-state assimilation (Farquhar *et al.*, 1980), conductance (Medlyn *et al.*, 2011), and energy balance model (Muir, 2019). The scaling of gas exchange from the leaf to the canopy is made using the Norman (1979) radiation model as implemented by Bonan (2019) to partition incoming radiation into direct and diffuse streams for each of 10 canopy layers. The gas exchange of the sun and shade leaves is then aggregated for each layer to calculate the canopy-scale A and E. Details regarding model parameters and equations used can be found in Lamour *et al.* (2023).

We ran the model at 1-h time increments from 15 May to 15 October 2021, using local meteorological data (Fig. 2). For all simulations, we modeled the canopy as being made up of 10 layers (Béland & Baldocchi, 2021), having a nonuniform, top-weighted distribution of LAI between layers (Bonan, 2015). LAI for each layer was scaled from the measured peak-season average (4.59 m^2 m^{-2}).

We ran two different versions of the model, one in which values of $V_{cmax.25}$, $R_{dark.25}$, g_0, and g_1 were consistent across the season, corresponding to the group average values (hereafter fixed model; Table 1), and a second model where values of $V_{cmax.25}$, $R_{dark.25}$, g_0, and g_1 were both month- and group-specific (hereafter variable model; Table S2). Other photosynthetic constants used in the model of photosynthesis (Farquhar *et al.*, 1980) can be found in Table S1. We investigated modeled results at a monthly interval and across the full season to compare the effect that model choice had on the estimation of E and NPP.

Stomatal limitation of assimilation

To estimate stomatal limitation on canopy assimilation, we reran the variable model, removing the effect of stomata by setting g_1 to infinity. This means that g_{sw} is unbounded from A, so for all rates of A, C_i is not a limiting factor. The resulting assimilation ($A_{infinite g_s}$) can be compared with the variable model estimate for assimilation ($A_{observed}$) to calculate stomatal limitation on net photosynthesis (I; Eqn 5; Farquhar & Sharkey, 1982; Long & Bernacchi, 2003; Slot & Winter, 2017).

$$I = 1 - \frac{A_{observed}}{A_{infinite g_s}} \quad \text{Eqn 5}$$

Here, a value of $I = 0$ represents no stomatal limitation on A (where $C_i = C_a$) while a value of $I = 1$ represents complete stomatal limitation on A.

Statistical analysis

To compare how estimates of $V_{cmax.25}$, $R_{dark.25}$, g_0, and g_1 varied across successive months, we used mixed effects models constructed and analyzed in the R package NLME (v.3.1; Pinheiro *et al.*, 2020). In total, we had 2681 observations of A and g_{sw}, collected from 240 individual leaves. For $V_{cmax.25}$, and $R_{dark.25}$, sampling site acted as the random effect, while for g_0, and g_1, which are both estimated from multiple nonindependent observations per leaf, both individual leaf and sampling site served as the random effect. For all data, we considered the species group and month of observation as fixed effects. We plotted the residual error relative to the group mean as a means of verifying that the two species in the maple and white oak groups were physiologically similar (Fig. S1).

We next used linear models to assess the assumed relationships between leaf-level traits (N_{area}, LMA, LDMC, stomatal density,

© 2023 The Authors.
New Phytologist © 2023 New Phytologist Foundation
This article has been contributed to by U.S. Government employees and their work is in the public domain in the USA.

14698137, 2023, 1, Downloaded from https://nph.onlinelibrary.wiley.com/doi/10.1111/nph.19137 by Columbia University Libraries, Wiley Online Library on [05/09/2024]. See the Terms and Conditions (https://onlinelibrary.wiley.com/terms-and-conditions) on Wiley Online Library for rules of use; OA articles are governed by the applicable Creative Commons License

RWD_{TLP}) and the leaf-level physiological parameters $V_{cmax.25}$, $R_{dark.25}$, g_0, and g_1. We also investigated whether linear relationships existed between different combinations of physiological parameters (e.g. a relationship between g_1 and $V_{cmax.25}$). We next used Spearman's rank correlation tests to investigate the relationships between monthly average meteorological variables and physiological parameters. To account for the increased probability of Type I error associated with multiple comparisons of the same parameter (12 comparisons per parameter), we applied a Bonferroni correction to adjust the α required to establish significance from the nominal value of 0.05–0.004 for both the linear models and the correlation tests. All analysis was performed using the R OPEN-SOURCE software environment (v.3.6.2, R Core Team, 2013).

Results

Seasonal patterns of leaf physiological parameters

We observed significant seasonal and group effects for all four parameters (Tables 1, S2). For most groups, $V_{cmax.25}$ exhibited a significant ($P < 0.05$) midseason peak rising to the highest rate in July before declining later in the season (Fig. 3a). The one exception to this pattern was maple, which displayed rates of $V_{cmax.25}$ that remained fairly constant through the season with no significant differences among months.

$R_{dark.25}$ showed a contrasting seasonal pattern to that of $V_{cmax.25}$ with high values at the beginning of the season and reaching a midseason minimum in either July (white oak) or August, before recovering to approximately half of the early season values by October (Fig. 3b). All four groups showed significant ($P < 0.001$) overall variation, with a significant decrease in estimated rates of $R_{dark.25}$ between May and the midsummer minimum in all four groups. The proportion of $R_{dark.25}$ to $V_{cmax.25}$ also varied considerably across the season, with the ratio reaching its maximum in either August or September for all groups (Fig. S2g).

Similar to $R_{dark.25}$, g_0 values for all four groups began the season at a peak before declining between June and September (Fig. 3d). This decline was significant ($P < 0.05$) for all four groups; however, birch remained variable between 0.88 and 1.88 μmol m^{-2} s^{-1}. For maple, there was a significant ($P < 0.05$) recovery of g_0 between August and October, as rates returned to *c.* 60% of their May values.

The g_1 for oak and maple increased significantly ($P < 0.001$) from an early season low to a peak in October (Fig. 3c). This pattern was most pronounced in red oak, which experienced a near tripling of g_1 (1.19–3.32 $kPa^{0.5}$) between June and October. Birch g_1 increased significantly ($P < 0.05$) between May and June; however, unlike the other groups, the g_1 value remained relatively constant for the remainder of the season.

Overall, when leaf gas exchange parameters were averaged over the full growing season, there was significant ($P < 0.001$) variation among groups for some traits (Table 1). $V_{cmax.25}$ was relatively consistent between groups, except for red oak which had a nonstatistically significant 40% higher rate. Birch and maple both exhibited significantly lower leaf respiration than the oaks. For the g_1 parameter, the species groups clustered into three groupings, with white oak and maple having significantly lower g_1 (higher WUE) than birch and red oak. Finally, birch differed from the other three groups, with a rate of g_0 nearly three times higher than the other groups.

In general, among-leaf variation for each given group was fairly consistent across successive months (Fig. 3). For the oak groups, $V_{cmax.25}$ varied the most among months, with a peak in July (Fig. 3a), while white oak displayed significant among-leaf variation in $R_{dark.25}$ in May and June (Fig. 3b). Among-leaf variation in g_1 and g_0 was comparable across all 6 months of study; however, birch exhibited substantially more leaf-to-leaf variation in g_0 than the other three groups (Fig. 3d).

Trait–trait and trait–environment relationships

Next, we examined the linear relationships between a suite of functional, structural, anatomical, and hydraulic leaf traits, which are assumed to explain some of the variation observed in the physiological parameters ($V_{cmax.25}$, $R_{dark.25}$, g_1, and g_0). We found a significant, yet weak ($R^2 = 0.23$) positive relationship between N_{area} and $V_{cmax.25}$ (Fig. 4a) and a slightly weaker ($R^2 = 0.18$) negative relationship between LMA and $V_{cmax.25}$ (Fig. 4c). The observed month-to-month variation in $R_{dark.25}$ was best explained by stomatal density ($R^2 = 0.45$; Fig. 4b) and LDMC ($R^2 = 0.44$; Fig. 4d); however, these relationships are primarily influenced by early season measurements on immature leaves when $R_{dark.25}$ was at its seasonal maximum. Neither the variation in $V_{cmax.25}$ nor $R_{dark.25}$ could be statistically explained by any of the hydraulic parameters tested.

Variation in stomatal parameters was less well explained by variation in traits with the only significant ($P < 0.004$) relationship observed between g_0 and the relative water deficit at turgor loss point ($R^2 = 0.71$, Fig. 5a). However, we found that variation in both $R_{dark.25}$ ($R^2 = 0.60$, Fig. 5d) and $V_{cmax.25}$ ($R^2 = 0.85$, Fig. 5b) explained some of the variation in g_1. In addition, g_0 was also linearly related to $R_{dark.25}$ ($R^2 = 0.67$, Fig. 5c). Seasonal variation in g_0 and g_1 could not be explained by Ψ_{TLP} or ε derived from PV curves.

Finally, we analyzed the relationships between the physiological parameters and five ambient environmental variables averaged by month: mean daytime (sunrise to sunset) irradiance, mean daytime temperature, mean daytime VPD, mean total 24-h precipitation, and mean 24-h soil moisture content (SMC; Fig. 6). Mean daytime temperature best explained variability in parameter estimates, with a positive relationship with $V_{cmax.25}$ ($\rho = 0.45$; Fig. 6e) and negative relationship with $R_{dark.25}$ ($\rho = -0.57$; Fig. 6f) and g_0 ($\rho = -0.65$; Fig. 6h). Mean daily irradiance also helped explain monthly variability in $R_{dark.25}$ ($\rho = 0.50$; Fig. 6b) and had a negative relationship with g_0 ($\rho = -0.49$; Fig. 6c). VPD, precipitation, and SMC were not significantly correlated with any of the four physiological parameters (Fig. 6i–t); however, there was a general positive relationship between SMC, g_0, and $R_{dark.25}$.

© 2023 The Authors.
New Phytologist © 2023 New Phytologist Foundation
This article has been contributed to by U.S. Government employees and their work is in the public domain in the USA.

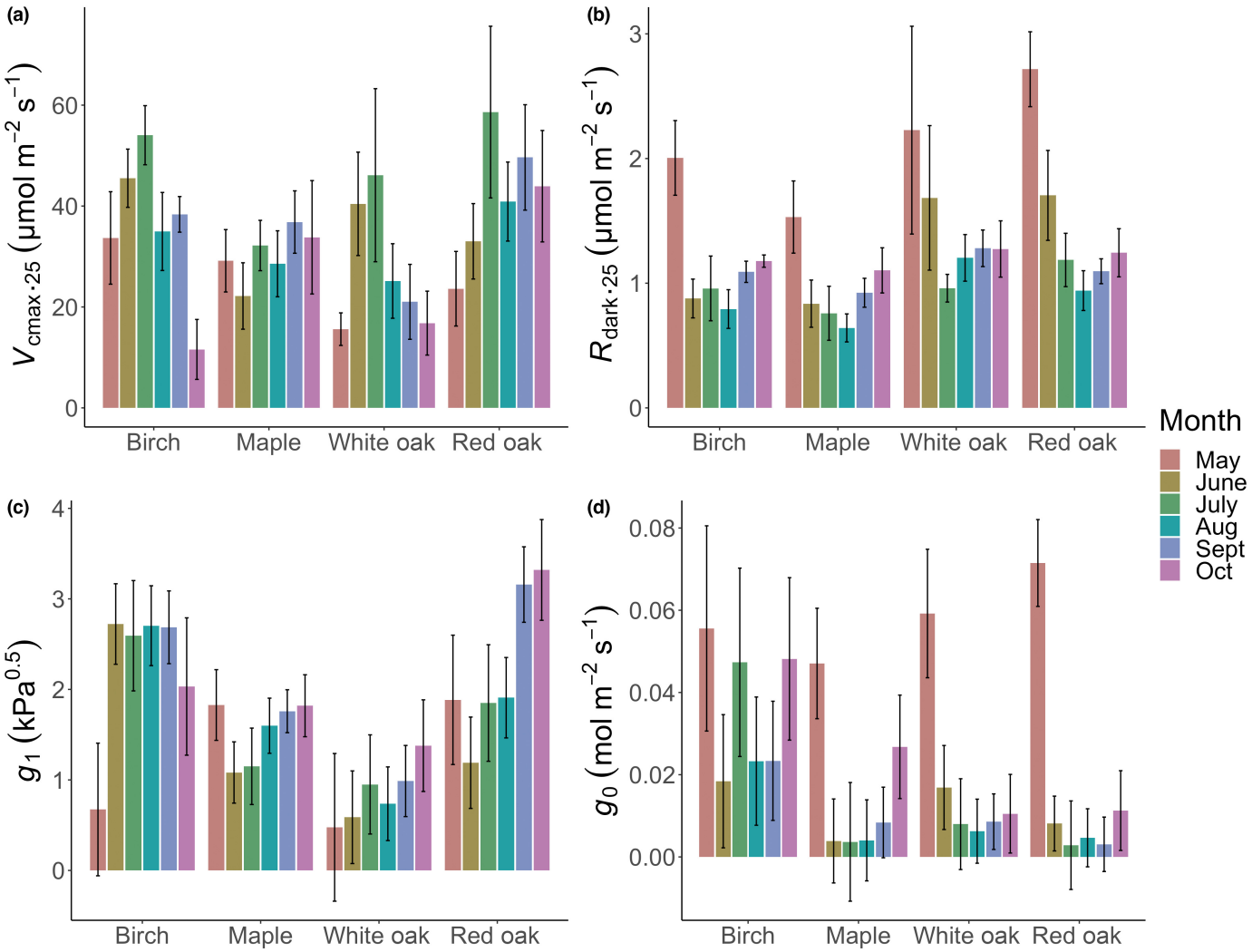


Fig. 3 Average monthly estimates of four important physiological parameters. (a) The maximum carboxylation capacity of Rubisco normalized to 25°C ($V_{cmax.25}$), (b) dark respiration rate normalized to 25°C ($R_{dark.25}$), (c) the stomatal slope parameter (g_1), and (d) stomatal intercept parameter (g_0) of the unified stomatal optimization model (Medlyn *et al*., 2011) measured throughout the growth season in four tree groups in the Black Rock Forest. Data shown are mean ± 2 SE (n = 9–12).

Model results

Our simulation of canopy E using a variable model parameterization (Fig. 7) resulted in a 63.4% higher rate of E in May compared with the fixed model, owing to the comparably poorer stomatal control of early season leaves (higher g_0 and lower g_1; Fig. 3c,d), compared with the full season average values of g_0 and g_1. Conversely, toward the middle and end of the growing season (August–September), rates of canopy E were 46.7% and 34% higher, respectively, for the model, which used fixed photosynthetic and stomatal parameters. Much of this variation is driven by the variable model having rates of $V_{cmax.25}$ that declined significantly and rates of $R_{dark.25}$ that increased significantly after the midseason growth peak in July (Figs 3a,b, S2g), while for the fixed model, $V_{cmax.25}$ and $R_{dark.25}$ were constant over the entire simulation period.

In our simulation of canopy A, we observed a similar effect to that of E, with the variable model predicting 53.7% lower mean canopy A in May (Fig. 8). This reduced rate of A in the variable model is the result of the significantly lower than average rate of $V_{cmax.25}$ and higher than average rate of $R_{dark.25}$ in May (Fig. 3a,b). The shape of the seasonal response was also different between the two models, with the variable model capturing a midseason peak in net assimilation while the fixed model predicted a progressive decline in net assimilation from the first 2 months to the end of the growth season (Fig. 8). Interestingly, this decline in the fixed model appeared to be driven solely by climatic factors such as ambient temperature and irradiance level, rather than a biotic or physiological process (Fig. 2).

When the two models are compared over the full 2021 growth season, accounting for the relative abundance of each group, it was possible to estimate total net assimilation and transpiration per unit ground area. The fixed parameter model estimates a 5-month total of 88.68 kg H_2O released and 1.67 kg CO_2 assimilated per meter of ground. The variable parameter model estimates a 5-month total of 103.05 kg H_2O released and 1.73 kg

© 2023 The Authors.
New Phytologist © 2023 New Phytologist Foundation
This article has been contributed to by U.S. Government employees and their work is in the public domain in the USA.

14698137, 2023, 1, Downloaded from https://nph.onlinelibrary.wiley.com/doi/10.1111/nph.19137 by Columbia University Libraries, Wiley Online Library on [05/09/2024]. See the Terms and Conditions (https://onlinelibrary.wiley.com/terms-and-conditions) on Wiley Online Library for rules of use; OA articles are governed by the applicable Creative Commons License

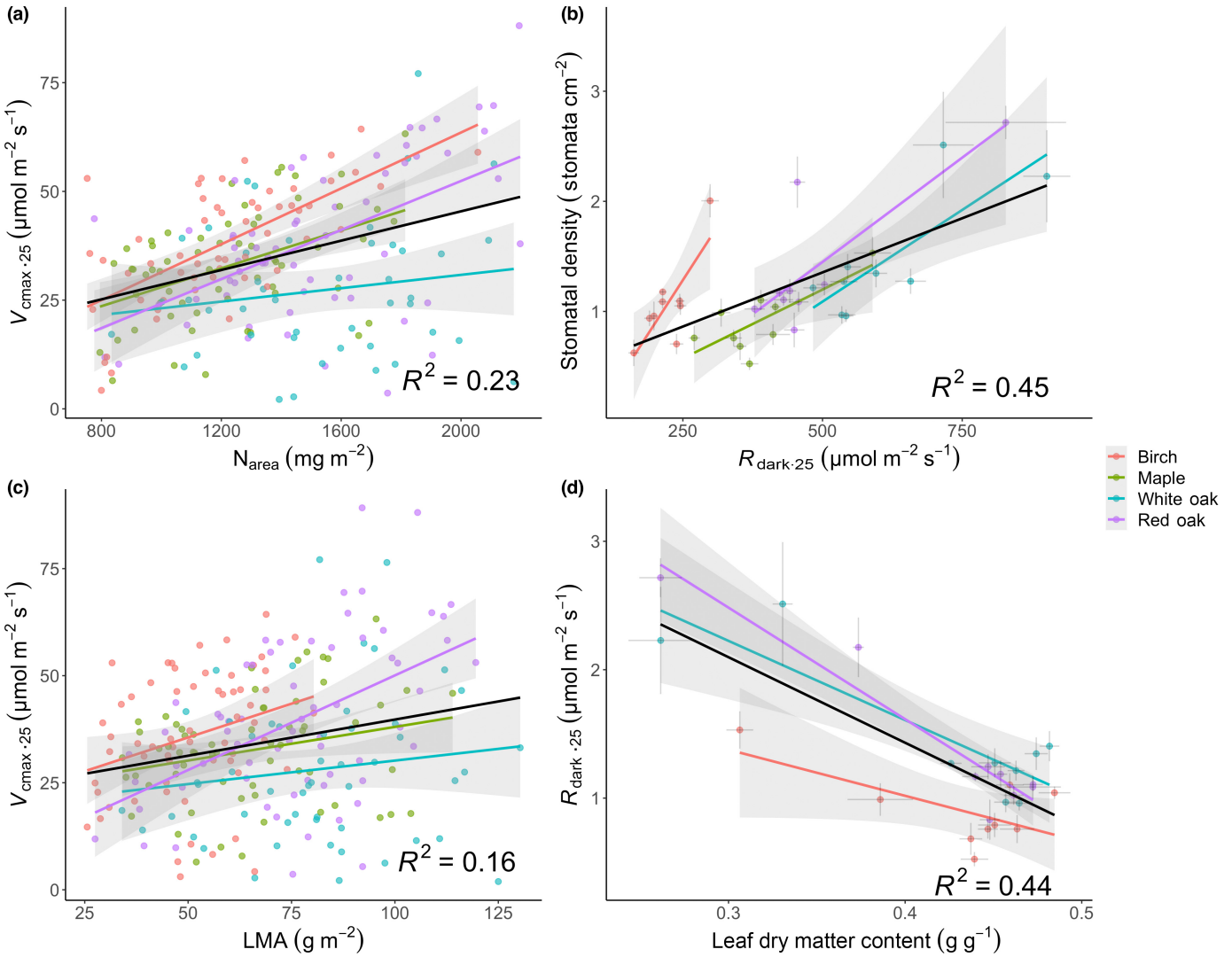


Fig. 4 Linear relationships between the maximum carboxylation capacity of Rubisco normalized to 25°C ($V_{cmax.25}$) and dark respiration rate normalized to 25°C ($R_{dark.25}$) and foliar functional traits. $V_{cmax.25}$ vs (a) foliar elemental nitrogen per unit area, and (c) leaf mass per area, and $R_{dark.25}$ vs (b) stomatal density and (d) leaf dry matter content. Points in (a) and (c) represent individual observations, while points in (b) and (d) are mean monthly observations with error bars ±2 SE (n = 9–12). Data for maple are excluded from (d) as the slope of the relationship was not significantly different from zero. Points to the extreme left in (d) and extreme right in (b) come from the start and end of the growth season. The black trend line is the overall relationship, while colored lines and shading around the lines are the species-group-specific relationships and prediction interval. All linear regressions shown are significant ($P < 0.004$).

CO_2 assimilated per meter of ground, values that are 16% and 3% higher, respectively, than the fixed model.

Finally, we can examine the degree to which g_{sw} limits A during model simulations (Table 2). A was most limited by g_{sw} in red oak (46.3% of observations), followed by maple (37.7%), white oak (25.4%), and birch (19.6%), and was most limited in July (56.6%) and least in October (2.7%). Stomatal limitation occurs more frequently in the afternoon than in the morning, with the highest average I calculated between 14:00 and 15:00 h (Fig. S3). All four groups appear to have equal diurnal distributions of I. Stomatal limitation is associated with periods of higher irradiance, VPD, and air temperature (Fig. S4) in all four groups; however, the strength of the association varies among groups. When we compare seasonal assimilation between the model with and without stomatal limitation, we find that on average, stomata limit potential assimilation by 10–20% (Fig. 9).

Discussion

We investigated the seasonal patterns of four physiological parameters, essential for accurate modeling of vegetation-atmosphere interactions and which are known or assumed to vary with leaf phenology. We sought to explore the biotic and abiotic factors associated with seasonal trends in physiological parameters and consider the effects that a time-varying parametrization would have on models of canopy E and A. Our results reveal a mid-growth season peak in $V_{cmax.25}$ for all four groups investigated, which coincides closely with the seasonal minimum in dark

© 2023 The Authors.
New Phytologist © 2023 New Phytologist Foundation
This article has been contributed to by U.S. Government employees and their work is in the public domain in the USA.

14698137, 2023, 1, Downloaded from https://nph.onlinelibrary.wiley.com/doi/10.1111/nph.19137 by Columbia University Libraries, Wiley Online Library on [05/09/2024]. See the Terms and Conditions (https://onlinelibrary.wiley.com/terms-and-conditions) on Wiley Online Library for rules of use; OA articles are governed by the applicable Creative Commons License

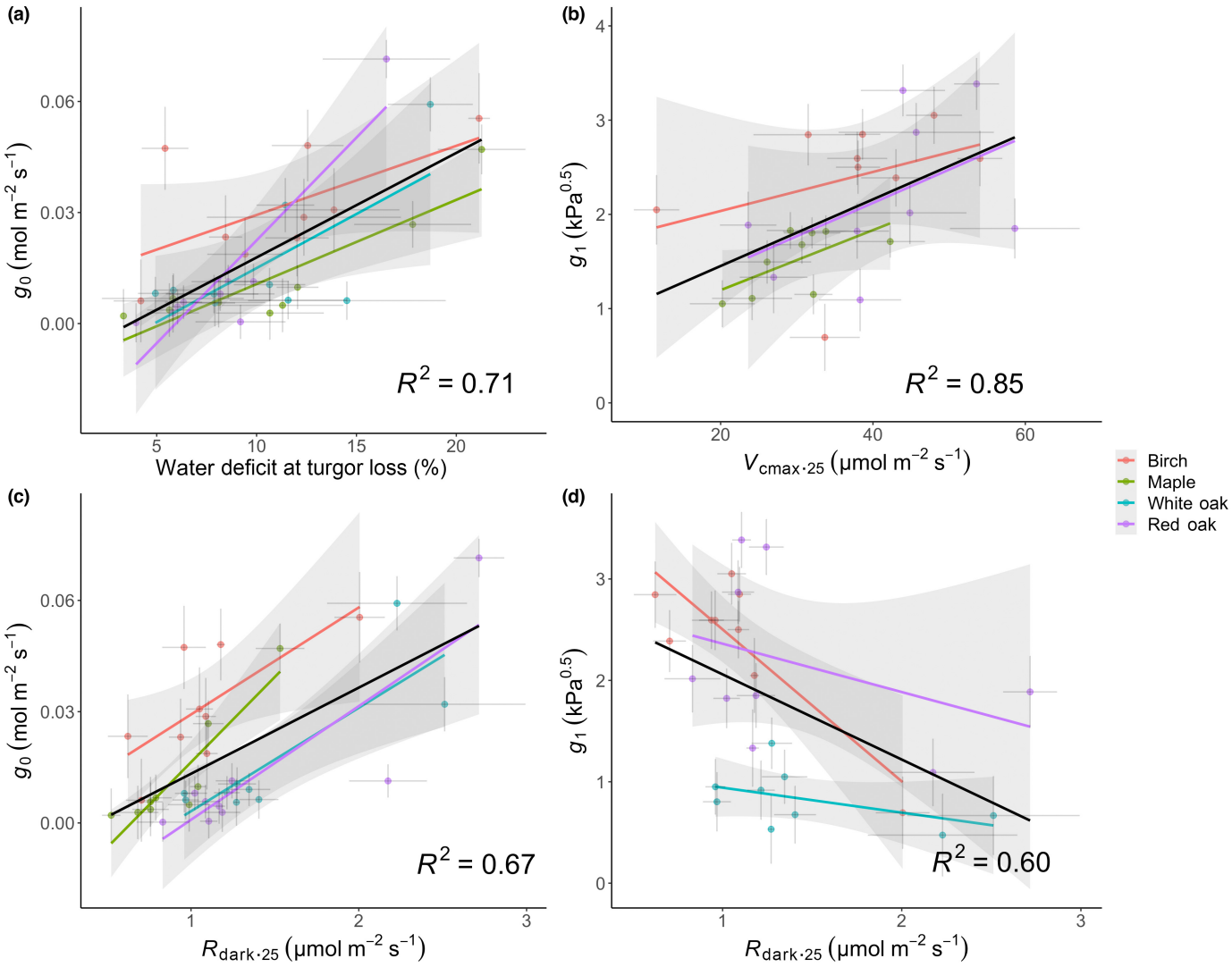


Fig. 5 Linear relationships between the stomatal intercept (g_0) and slope parameter (g_1) from the unified stomatal optimization model (Medlyn *et al*., 2011) and foliar photosynthetic and hydraulic traits. g_0 vs (a) relative water deficit at the point of turgor loss, and (c) dark respiration rate normalized to 25°C ($R_{dark.25}$), and g_1 vs (b) the maximum carboxylation capacity of Rubisco normalized to 25°C ($V_{cmax.25}$) and (d) $R_{dark.25}$. Points are mean monthly observations with error bars ±2 SE (n = 9–12 see Supporting Information Table S2 for further details). The black trend line is the overall relationship, while colored lines and shading around the line are the species-group-specific relationships and prediction interval. All linear regressions shown are significant ($P < 0.004$).

respiration rate (Fig. 3a,b), while g_1 progressively decreased over the season in three of the four groups (Fig. 3c). Photosynthetic parameters closely track seasonal trends in leaf structural, nutritional, and anatomical characteristics (Fig. 4), while stomatal parameters are correlated most strongly with changes in the $V_{cmax.25}$ and the relative water deficit at the point of turgor loss (Fig. 5). Furthermore, the lack of coordination between $V_{cmax.25}$ and maximum stomatal conductance (g_{swmax}) as evidenced by dynamic stomatal limitation across leaf phenology (Table 2) suggests that the seasonal dynamics of WUE observed here are the result of variable stomatal behavior, rather than a passive stomatal response to changes in assimilation potential. Our simulations indicate that there is a clear need for models to more explicitly account for seasonality in both photosynthetic and stomatal parameters for temperate broadleaf deciduous forest species (Figs 7, 8). We show that over the full 2021 season, the model with a time-varying parametrization results in a 16% higher cumulative E and a 3% higher cumulative A (Fig. 9) with differences most pronounced in the shoulder seasons (e.g. spring leaf flush), which are expected to be strongly impacted by climate change.

Seasonal variability and ontogenetic controls of photosynthetic capacity

The photosynthetic parameters $V_{cmax.25}$ and $R_{dark.25}$ displayed a strong seasonality across the 2021 growth season for all four groups studied (Fig. 3a,b). This is comparable to other studies in

© 2023 The Authors.
New Phytologist © 2023 New Phytologist Foundation
This article has been contributed to by U.S. Government employees and their work is in the public domain in the USA.

14698137, 2023, 1, Downloaded from https://nph.onlinelibrary.wiley.com/doi/10.1111/nph.19137 by Columbia University Libraries, Wiley Online Library on [05/09/2024]. See the Terms and Conditions (https://onlinelibrary.wiley.com/terms-and-conditions) on Wiley Online Library for rules of use; OA articles are governed by the applicable Creative Commons License

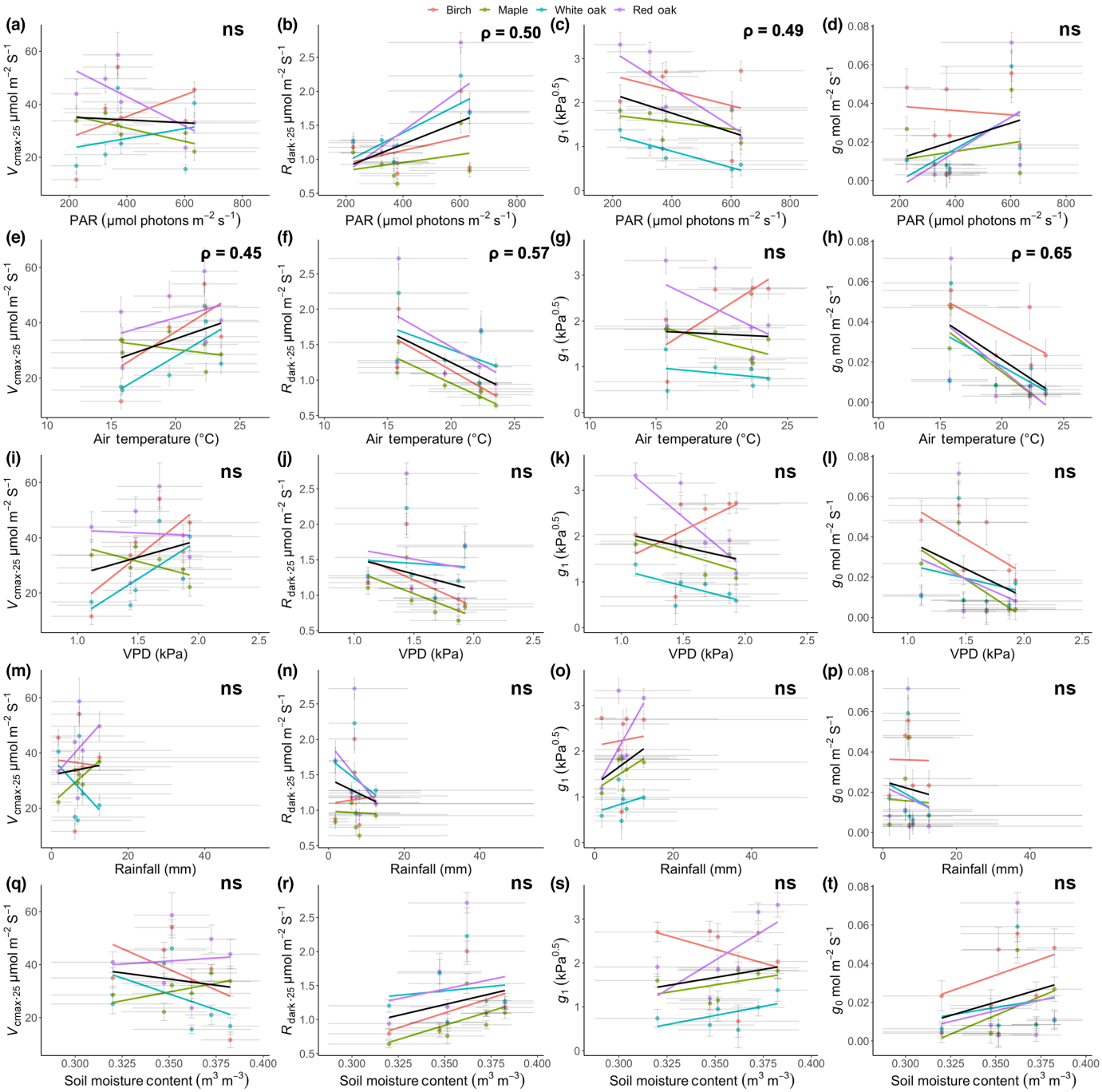


Fig. 6 Relationships between monthly mean meteorological conditions (daytime PAR (a–d), daytime air temperature (e–h), daytime VPD (i–l), total 24-h total precipitation (m–p), and 24-h soil moisture content (q–t)) and monthly mean physiological traits (the maximum carboxylation capacity of Rubisco normalized to 25°C ($V_{cmax.25}$), the dark respiration rate normalized to 25°C ($R_{dark.25}$), the stomatal slope parameter (g_1), and the stomatal intercept parameter (g_0) of the unified stomatal optimization model) by species group. Points represent monthly average estimates with error bars ±2 SE. The black trend line is the overall relationship, while colored lines are species-group-specific relationships. Values for the Spearman's rank correlation coefficient (ρ) in each panel represent the overall correlation (ns, not significant; $P < 0.004$).

eastern deciduous forests (Wehr *et al.*, 2016; Yang *et al.*, 2020), where $V_{cmax.25}$ followed a peaked response, with a peak slightly after the summer solstice (Figs 2a, 3a) at the period of full leaf expansion. While the seasonal maximum in $V_{cmax.25}$ did not correspond with the maximum day length or maximum daily irradiance (Fig. 2a) as has been demonstrated previously (Wilson *et al.*, 2000a, 2001; Grassi *et al.*, 2005; Bauerle *et al.*, 2012), it did correspond to the period of highest daytime air temperature and VPD (Fig. 2b,c). This is a similar seasonal pattern observed in previous studies of temperate ecosystems (Medvigy *et al.*, 2013; Luo *et al.*, 2021) in which daytime air temperature was the strongest determinant of ecosystem productivity and

© 2023 The Authors.
New Phytologist © 2023 New Phytologist Foundation
This article has been contributed to by U.S. Government employees and their work is in the public domain in the USA.

14698137, 2023, 1, Downloaded from https://nph.onlinelibrary.wiley.com/doi/10.1111/nph.19137 by Columbia University Libraries, Wiley Online Library on [05/09/2024]. See the Terms and Conditions (https://onlinelibrary.wiley.com/terms-and-conditions) on Wiley Online Library for rules of use; OA articles are governed by the applicable Creative Commons License

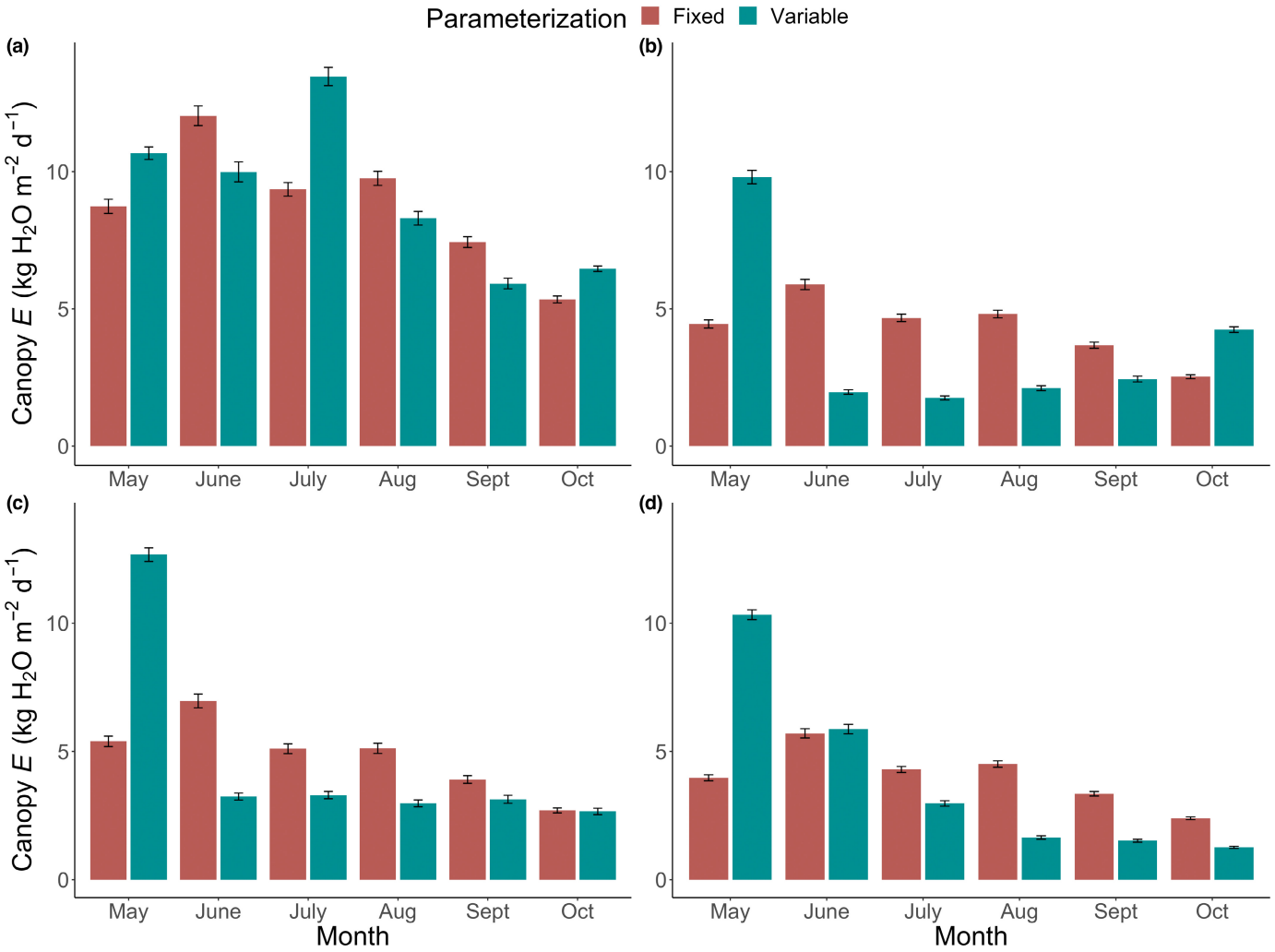


Fig. 7 Model estimates for total monthly canopy transpiration using two different model parametrizations. (a) Birch, (b) maple, (c) red oak, and (d) white oak. In the fixed model, values for the four key physiological parameters (the maximum carboxylation capacity of Rubisco normalized to 25°C ($V_{cmax.25}$), the dark respiration rate normalized to 25°C ($R_{dark.25}$), the stomatal slope parameter (g_1), and the stomatal intercept parameter (g_0) of the unified stomatal optimization model) are the same between months. In the variable model, physiological parameters are month specific. Error bars are ±2 SE of the mean monthly estimate ($n = 30$–31).

photosynthetic capacity. Consistent precipitation and SMC over the growth season (Fig. 2d,e) may also contribute to the lack of a seasonal decline in $V_{cmax.25}$ as has been observed in studies of drought-prone ecosystems (Bauerle *et al.*, 2012; Zhou *et al.*, 2014; Gourlez de la Motte *et al.*, 2020; Granda *et al.*, 2020). Of the five meteorological variables investigated here, mean daytime air temperature best explained seasonal progression of $V_{cmax.25}$ and $R_{dark.25}$ (Fig. 6e,f). This tight coupling between $V_{cmax.25}$ and $R_{dark.25}$ is expected given that the enzyme Rubisco constitutes a considerable proportion of total foliar protein (Amthor, 2000; Atkin *et al.*, 2000; Cannell, 2000; O'Leary *et al.*, 2019), and recently both $V_{cmax.25}$ and $R_{dark.25}$ were shown to acclimate in unison to changes in growth temperature (Wang *et al.*, 2020). However, here we observed a ratio of $R_{dark.25}$ to $V_{cmax.25}$ which is seasonally dynamic (Fig. S2g), calling into question the long-held model assumption that $R_{dark.25}$ should be *c.* 1.5% of $V_{cmax.25}$ (Collatz *et al.*, 1991).

In addition to abiotic conditions, several biotic traits also showed a significant correlation with photosynthetic capacity. This included a linear relationship between both N_{area} and LMA and $V_{cmax.25}$ (Fig. 3a,c). Like $V_{cmax.25}$, N_{area} peaked in the middle of the summer (Fig. S2d), which is unsurprising given the often observed linear relationship between foliar nitrogen content and $V_{cmax.25}$ (Ellsworth & Reich, 1993; Misson *et al.*, 2006; Rogers, 2014; Evans & Clarke, 2019). LMA increased rapidly from May to June and continued to increase to a maximum value at the end of the season, just before senescence (Fig. S2a), in agreement with previous literature suggesting a strong positive relationship between seasonal phenology and LMA (Grassi *et al.*, 2005; Wright *et al.*, 2006; Hikosaka *et al.*, 2007), and also observed in similar deciduous forests located in the northeastern United States (Yang *et al.*, 2016). This linear relationship between $V_{cmax.25}$, N_{area}, and LMA suggests that not only are these relationships robust across leaf ontogeny but also that nitrogen

© 2023 The Authors.
New Phytologist © 2023 New Phytologist Foundation
This article has been contributed to by U.S. Government employees and their work is in the public domain in the USA.

14698137, 2023, 1, Downloaded from https://nph.onlinelibrary.wiley.com/doi/10.1111/nph.19137 by Columbia University Libraries, Wiley Online Library on [05/09/2024]. See the Terms and Conditions (https://onlinelibrary.wiley.com/terms-and-conditions) on Wiley Online Library for rules of use; OA articles are governed by the applicable Creative Commons License

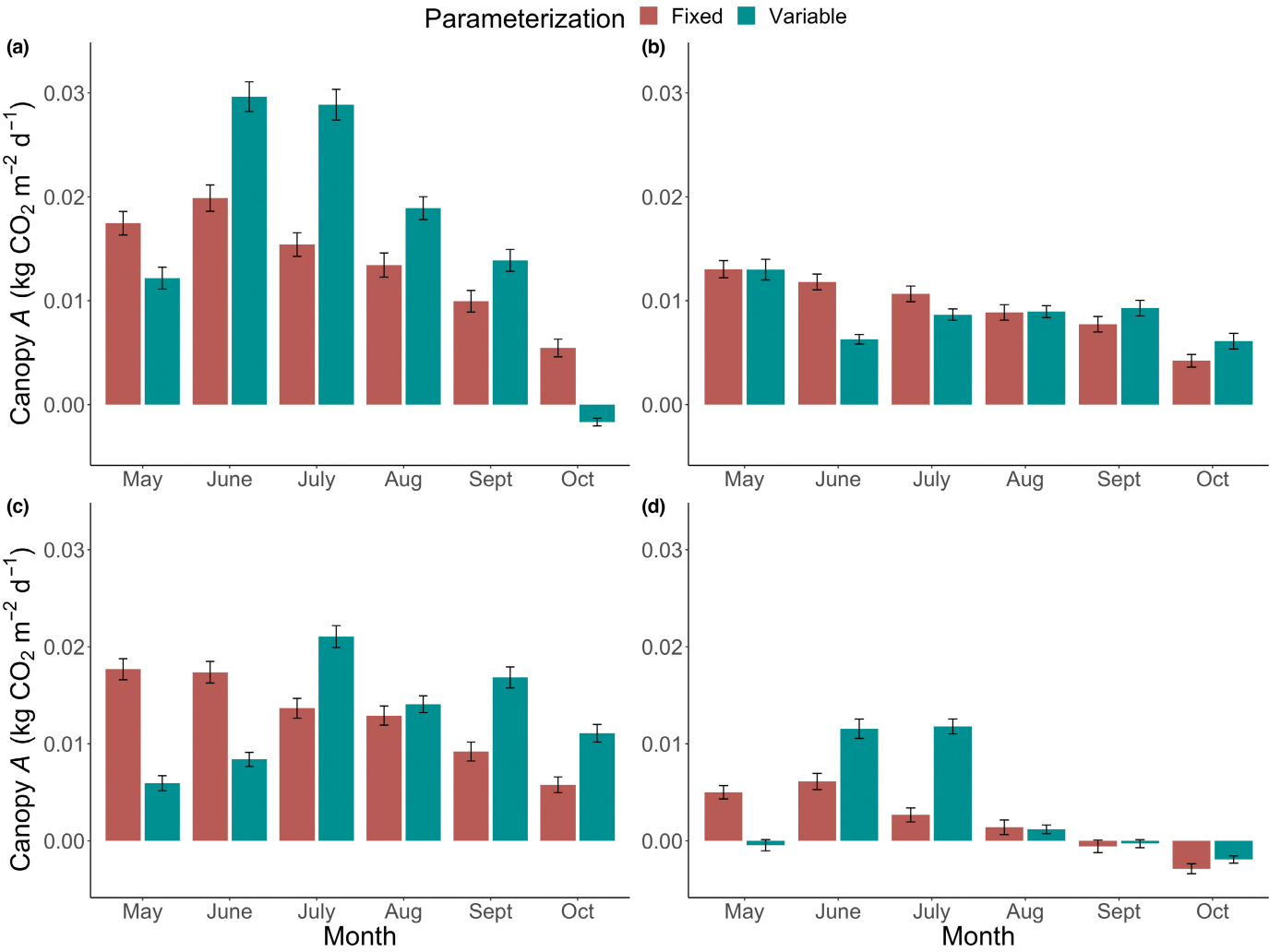


Fig. 8 Model estimates for total monthly canopy net carbon assimilation using two different model parametrizations. (a) birch, (b) maple, (c) red oak, and (d) white oak. In the fixed model, values for the four key physiological parameters (the maximum carboxylation capacity of Rubisco normalized to 25°C ($V_{cmax.25}$), the dark respiration rate normalized to 25°C ($R_{dark.25}$), the stomatal slope parameter (g_1), and the stomatal intercept parameter (g_0) of the unified stomatal optimization model) are the same between months. In the variable model, physiological parameters are month specific. Error bars are ±2 SE of the mean monthly estimate ($n = 30–31$).

use efficiency is constant across the growth season (Wilson *et al.*, 2001).

We also observed a positive linear relationship between stomatal density and $R_{dark.25}$ (Fig. 4b), with both traits reaching seasonal minimums in midsummer, after full leaf expansion. Interestingly however, we found no significant relationship between stomatal density and g_1, g_0, or g_{swmax}, all three of which have been extensively documented in previous among-species studies of natural vegetation and cultivated crops (Franks *et al.*, 2009; Franks & Beerling, 2009; Bertolino *et al.*, 2019; Machado *et al.*, 2021). The lack of a within-species link between stomatal density and stomatal parameters, along with the relationship between stomatal density and $R_{dark.25}$, suggests that these changes, while both associated with leaf ontogeny, themselves may not be causally linked. Finally, we observed a negative relationship between $R_{dark.25}$ and LDMC (Fig. 4d), a relationship widely reported in studies of the global leaf economic spectrum (LES; Wright *et al.*, 2004; Reich, 2014).

Seasonal variability and ontogenetic controls of stomatal behavior

In this study, we found that I, which is associated with higher air temperatures and VPD (Fig. S3i–l), is highest in the middle of the season, declining as leaves senesce (Table 2). Likewise, we observed a seasonal decline in foliar WUE (increasing g_1, Fig. 3c) in three of four groups. Several previous studies of other deciduous species (e.g. Wilson *et al.*, 2000b; Xu & Baldocchi, 2003; Grassi & Magnani, 2005) have observed contrasting trends, such as increasing I and decreasing or stable WUE throughout the season. However, the three above studies occurred in warm climates, with a pronounced seasonal drought effect, and in one case (Xu

© 2023 The Authors.
New Phytologist © 2023 New Phytologist Foundation
This article has been contributed to by U.S. Government employees and their work is in the public domain in the USA.

14698137, 2023, 1, Downloaded from https://nph.onlinelibrary.wiley.com/doi/10.1111/nph.19137 by Columbia University Libraries, Wiley Online Library on [05/09/2024]. See the Terms and Conditions (https://onlinelibrary.wiley.com/terms-and-conditions) on Wiley Online Library for rules of use; OA articles are governed by the applicable Creative Commons License

14698137, 2023, 1, Downloaded from https://nph.onlinelibrary.wiley.com/doi/10.1111/nph.19137 by Columbia University Libraries, Wiley Online Library on [05/09/2024]. See the Terms and Conditions (https://onlinelibrary.wiley.com/terms-and-conditions) on Wiley Online Library for rules of use; OA articles are governed by the applicable Creative Commons License

Table 2 Estimates of monthly mean stomatal limitation on photosynthesis (l) and the proportions of observations (1-h model timestep) where limitation occurs.

Group	Month	Mean value of l	Proportion of observations $l > 0$ (%)
Birch	May	0.221	7.2
	June	0.231	32.0
	July	0.086	24.1
	August	0.142	31.9
	September	0.087	10.3
	October	–	0.0
Maple	May	0.208	20.5
	June	0.374	61.3
	July	0.240	58.7
	August	0.306	52.1
	September	0.177	15.0
	October	0.168	3.3
White oak	May	0.418	3.9
	June	0.221	39.8
	July	0.103	62.1
	August	0.201	22.9
	September	0.268	0.7
	October	–	0.0
Red oak	May	0.177	23.9
	June	0.276	63.0
	July	0.163	83.2
	August	0.191	65.8
	September	0.174	19.7
	October	0.128	6.6

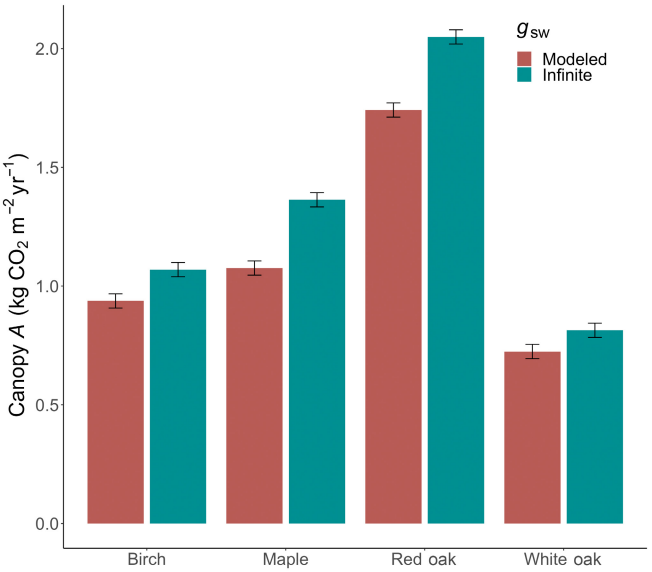


Fig. 9 Total canopy net assimilation per unit ground area, for four of the most common species groups present at Black Rock Forest. Bars in blue represent a model run when g_1 was set to infinity, removing stomatal limitation on potential assimilation. Bars in red represent the standard variable model run. Error bars are ±2 SE of the mean.

& Baldocchi, 2003) focused on a drought-adapted species, a strong contrast with the seasonally cold and wet conditions present at BRF (Fig. 2). The presence of a seasonal decline in WUE is not without some established support. In similar forests to BRF, both Sang *et al.* (2011) and Burnett *et al.* (2021) observed a seasonal decline in WUE, with an early season maximum and late season minimum. The seasonal shifts in WUE observed here may be driven by ontogenetic processes, such as a seasonal shift from conservative stomatal behavior to protect new vegetation (Gimeno *et al.*, 2019) toward more profligate behavior to maximize carbon assimilation before leaf senescence (Brodribb & Holbrook, 2003; Sanchez *et al.*, 2013; Burnett *et al.*, 2021).

Previous studies (De Kauwe *et al.*, 2015; Duursma *et al.*, 2019) have called into question the biophysical interpretation of the g_0 parameter, suggesting that depending upon the method used to derive it, it may represent error in fitting rather than an actual biological trait. However, in this study we measure the full response of stomatal conductance to changes in irradiance above and below the light compensation point (Fig. 1d), which enables us to observe actual daytime rates of g_{sw} at and around g_0. While g_0 is not predicted by optimality theory (Cowan & Fraquhar, 1977), g_0 nonetheless represents a true biophysical parameter with a mechanism similar to minimum conductance, the lower bound of the possible range of g_{sw} (Duursma *et al.*, 2019). The g_0 measured in this study can be interpreted as a mechanistic parameter representing water loss both from the cuticular pathway (Márquez *et al.*, 2021, 2022) and from incomplete stomatal closure (Machado *et al.*, 2021) when A_n is zero. Thus, seasonal changes in g_0 reflect seasonal changes in the rate of water loss from the leaf during conditions when photosynthesis is no longer leading to net carbon gain.

Leaf ontogenetic changes may influence the patterns of g_0 we observed, which have been observed in other studies of oak species (Granda *et al.*, 2020). During the first measurement period, all four groups had a markedly higher g_0 (up to 8×) than their respective midseason average. Recent evidence from a study of red oaks suggests that the majority of this early season foliar water loss comes from cuticular leakage in immature leaves, rather than lack of stomatal control (Kane *et al.*, 2020). The small uptick in g_0 observed in October may be the result of the onset of leaf senescence, which has long been associated with a decrease in stomatal control (Gee & Federer, 1972; Wardle & Short, 1983).

The seasonal patterns of g_1 and g_0 observed in this study may be partially explained by the seasonal progression of climate factors (Fig. 2). In all four groups, g_1 declined linearly as a function of mean daytime irradiance (Fig. 6c), while g_0 declined with increasing mean daytime air temperature (Fig. 6h). Interestingly, monthly trends of VPD and precipitation were not significantly correlated with either g_1 or g_0, while monthly SMC showed a weak, yet nonsignificant, positive association with g_0 (Fig. 6t). This latter finding, however, may have more to do with the mesic conditions at the start and end of the growing season when g_0 was higher. The overall trends in g_0 and g_1 we observed run in contrast to predictions of hydraulic theory (Martínez-Vilalta & Garcia-Forner, 2017; Anderegg, 2018), which suggests that periods of drought and high VPD, especially toward leaf senescence (Pantin *et al.*, 2012) should reduce Ψ_{leaf}, and thus reduce g_1 and g_0. However, during the study VPD, precipitation, and SMC remained relatively consistent across the season (i.e. no major periods of drought) and do not appear to have an impact on predawn Ψ_{leaf} (Fig. S5b). We did observe a positive relationship

© 2023 The Authors.
New Phytologist © 2023 New Phytologist Foundation
This article has been contributed to by U.S. Government employees and their work is in the public domain in the USA.

between g_0 and the relative water deficit at the turgor loss point (RWD_{TLP}, Fig. 5a), suggesting a potential water stress mitigation strategy, as leaves which lose more water at or below net-zero assimilation require more relative water loss before losing turgidity. Seasonal patterns of RWD_{TLP} follow the same pattern as predawn Ψ_{leaf} (Fig. S5), reinforcing the adaptive role stomata play in buffering against the risk of hydraulic damage (Bartlett *et al.*, 2016).

Monthly mean g_1 and g_0 also exhibited linear relationships with photosynthetic parameters (Fig. 5b,d). Most notably, g_1 was positively associated with $V_{cmax.25}$, and negatively associated with $R_{dark.25}$. It has long been assumed that a tight coordination between rates of A and g_{sw} results in a fixed ratio of $C_i : C_a$, even as photosynthetic capacity changes (Wong *et al.*, 1979, 1985; McDowell *et al.*, 2006), as although $V_{cmax.25}$ may shift with leaf phenology, the rate of g_{sw} will change in proportion to supply and maintain a stable level of intercellular CO_2 (Long & Hällgren, 1993). These changes also have the effect of reducing the potential for g_{sw} to limit A (Drake *et al.*, 2017). If present, a coordination between $V_{cmax.25}$ and g_{swmax} would result in stable g_1 and I across leaf phenology; however, our data, and that of a similar study (Burnett *et al.*, 2021), do not support such a coordination. This suggests that the seasonal dynamics of WUE observed here are the result of dynamic stomatal behavior, rather than a passive stomatal response to changes in assimilation potential.

Implications for land-surface modeling

Applying our findings of the seasonality in $V_{cmax.25}$, $R_{dark.25}$, g_1, and g_0 significantly altered model output for both E and A (Figs 7, 8), consistent with other studies that considered the effect of seasonality in models (Wang *et al.*, 2004; Bauerle *et al.*, 2012; Medvigy *et al.*, 2013; Burnett *et al.*, 2021). Our model parameterization differs somewhat from other studies, both in how we chose to apply seasonality and the values we used for our fixed model. Both Bonan *et al.* (2011) and Burnett *et al.* (2021) use a maximum or solstice value for $V_{cmax.25}$ in their model without seasonality, which results in a seasonal model with a value of $V_{cmax.25}$ which is always less than or equal to the nonseasonal model. Unsurprisingly, Bonan *et al.* (2011) found that implementing seasonality reduced NPP by *c.* 8%, while Burnett *et al.* (2021) found a smaller, yet still significant effect of seasonality which reduced cumulative canopy A. Medvigy *et al.* (2013) applied a function scaling $V_{cmax.25}$ based on photoperiod and found that simulating seasonality resulted in a 3% increase in NPP, the same increase to A as we observed in this study.

Unlike previous studies, which have primarily focused on the impact of seasonality on carbon assimilation, we were also interested in the effect that a variable g_1 and g_0 would have on seasonal simulations of E. The use of variable stomatal parameters reveals a substantial underestimation of early season E compared with the fixed model (Fig. 7), leading to a 16% higher total seasonal transpiration rate for the variable model than the fixed model. We also observe that stomatal limitation on A plays a small yet significant role in regulating seasonal assimilation, on average reducing potential A by 10–20% (Fig. 9), reinforcing the importance of appropriate estimation of stomatal parameters in earth system modeling (De Kauwe *et al.*, 2015).

Based on the findings presented in this study and others (e.g. Medvigy *et al.*, 2013; Burnett *et al.*, 2021), there is a clear need for models to account for seasonality in both photosynthetic and stomatal parameters, with emphasis given toward ensuring that photosynthetic and stomatal parameters correctly scale with one another. The increasing development of models which predict physiology according to climatic optimality principles (Smith *et al.*, 2019; Caldararu *et al.*, 2020; Cooley *et al.*, 2022) provides an opportunity for the modeling community to move away from models, which use a seasonal mean value or fixed model parameters. While our study provides a semiempirical model at a single site for a single season, we nonetheless advocate for future studies which move toward a true mechanistic representation of how parameters, at the intersection of leaf ontogeny and climate, change seasonally. Accomplishing a reparameterization of models will be a difficult task, yet one which will substantially improve our understanding of land–atmosphere interactions across diverse geographical regions and variable environmental conditions.

Acknowledgements

We would like to thank the Black Rock Forest Consortium for the use of their field site, logistical support, and funding for this project in the form of the David Redden Conservation Science Fund. Additional funding was provided by Stony Brook University, Department of Ecology and Evolution, through the Lawrence B. Slobodkin Research Fund, and the Next-Generation Ecosystem Experiments–Tropics project supported by the US DOE, Office of Science, Office of Biological and Environmental Research, and through the United States Department of Energy contract no. DE-SC0012704 to Brookhaven National Laboratory.

Competing interests

None declared.

Author contributions

KJD and SPS conceived and designed the study. KJD, SPS, JL and AM contributed to methodology development, experiment execution and data collection. KJD, SPS, JL and AR analyzed the data. KJD wrote the manuscript with contributions from all authors.

ORCID

Kenneth J. Davidson https://orcid.org/0000-0001-5745-9689
Julien Lamour https://orcid.org/0000-0002-4410-507X
Anna McPherran https://orcid.org/0000-0001-8157-7642
Alistair Rogers https://orcid.org/0000-0001-9262-7430
Shawn P. Serbin https://orcid.org/0000-0003-4136-8971

© 2023 The Authors.
New Phytologist © 2023 New Phytologist Foundation
This article has been contributed to by U.S. Government employees and their work is in the public domain in the USA.

14698137, 2023, 1, Downloaded from https://nph.onlinelibrary.wiley.com/doi/10.1111/nph.19137 by Columbia University Libraries, Wiley Online Library on [05/09/2024]. See the Terms and Conditions (https://onlinelibrary.wiley.com/terms-and-conditions) on Wiley Online Library for rules of use; OA articles are governed by the applicable Creative Commons License

14698137, 2023, 1, Downloaded from https://nph.onlinelibrary.wiley.com/doi/10.1111/nph.19137 by Columbia University Libraries, Wiley Online Library on [05/09/2024]. See the Terms and Conditions (https://onlinelibrary.wiley.com/terms-and-conditions) on Wiley Online Library for rules of use; OA articles are governed by the applicable Creative Commons License

Data availability

All data in support of this study are publicly available through the EDI Data Repository in the data package: doi: 10.6073/pasta/400eae2df484707ced77d2c2563e3c6c (Davidson *et al.*, 2023).

References

Ali AA, Xu C, Rogers A, McDowell NG, Medlyn BE, Fisher RA, Wullschleger SD, Reich PB, Vrugt JA, Bauerle WL *et al.* 2015. Global-scale environmental control of plant photosynthetic capacity. *Ecological Applications* **25**: 2349–2365.

Amthor J. 2000. The McCree–de Wit–Penning de Vries–Thornley respiration paradigms: 30 years later. *Annals of Botany* **86**: 1–20.

Anderegg WRL. 2018. Quantifying seasonal and diurnal variation of stomatal behavior in a hydraulic-based stomatal optimization model. *Journal of Plant Hydraulics* **5**: e001.

Atkin OK, Millar AH, Gardeström P, Day DA. 2000. Photosynthesis, carbohydrate metabolism and respiration in leaves of higher plants. In: Leegood RC, Sharkey TD, von Caemmerer S, eds. *Photosynthesis*. Dordrecht, the Netherlands: Springer, 153–175.

Ball TJ, Woodrow IE, Berry JA. 1987. A model predicting stomatal conductance and its contribution to the control of photosynthesis under different environmental conditions. In: Biggins J, ed. *Progress in photosynthesis research*. Dordrecht, the Netherlands: Springer, 221–224.

Bartlett MK, Klein T, Jansen S, Choat B, Sack L. 2016. The correlations and sequence of plant stomatal, hydraulic, and wilting responses to drought. *Proceedings of the National Academy of Sciences, USA* **113**: 13098–13103.

Bartlett MK, Scoffoni C, Sack L. 2012. The determinants of leaf turgor loss point and prediction of drought tolerance of species and biomes: a global meta-analysis: drivers of plant drought tolerance. *Ecology Letters* **15**: 393–405.

Bauerle WL, Oren R, Way DA, Qian SS, Stoy PC, Thornton PE, Bowden JD, Hoffman FM, Reynolds RF. 2012. Photoperiodic regulation of the seasonal pattern of photosynthetic capacity and the implications for carbon cycling. *Proceedings of the National Academy of Sciences, USA* **109**: 8612–8617.

Béland M, Baldocchi DD. 2021. Vertical structure heterogeneity in broadleaf forests: effects on light interception and canopy photosynthesis. *Agricultural and Forest Meteorology* **307**: 108525.

Bernacchi CJ, Bagley JE, Serbin SP, Ruiz-Vera UM, Rosenthal DM, Vanloocke A. 2013. Modelling C_3 photosynthesis from the chloroplast to the ecosystem: scaling photosynthesis using models. *Plant, Cell & Environment* **36**: 1641–1657.

Bernacchi CJ, Singsaas EL, Pimentel C, Portis AR Jr, Long SP. 2001. Improved temperature response functions for models of Rubisco-limited photosynthesis: *in vivo* Rubisco enzyme kinetics. *Plant, Cell & Environment* **24**: 253–259.

Bertolino LT, Caine RS, Gray JE. 2019. Impact of stomatal density and morphology on water-use efficiency in a changing world. *Frontiers in Plant Science* **10**: 225.

Blyth EM, Arora VK, Clark DB, Dadson SJ, De Kauwe MG, Lawrence DM, Melton JR, Pongratz J, Turton RH, Yoshimura K *et al.* 2021. Advances in land surface modelling. *Current Climate Change Reports* **7**: 45–71.

Bonan G. 2015. *Ecological climatology: concepts and applications*. Cambridge, UK: Cambridge University Press.

Bonan G. 2019. *Climate change and terrestrial ecosystem modeling*. Cambridge, UK: Cambridge University Press.

Bonan GB, Lawrence PJ, Oleson KW, Levis S, Jung M, Reichstein M, Lawrence DM, Swenson SC. 2011. Improving canopy processes in the Community Land Model v.4 (CLM4) using global flux fields empirically inferred from FLUXNET data. *Journal of Geophysical Research* **116**: G02014.

Brodribb TJ, Holbrook NM. 2003. Stomatal closure during leaf dehydration, correlation with other leaf physiological traits. *Plant Physiology* **132**: 2166–2173.

Burnett AC, Davidson KJ, Serbin SP, Rogers A. 2019. The "one-point method" for estimating maximum carboxylation capacity of photosynthesis: a cautionary tale. *Plant, Cell & Environment* **42**: 2472–2481.

Burnett AC, Serbin SP, Lamour J, Anderson J, Davidson KJ, Yang D, Rogers A. 2021. Seasonal trends in photosynthesis and leaf traits in scarlet oak. *Tree Physiology* **41**: 1413–1424.

von Caemmerer S, Farquhar GD. 1981. Some relationships between the biochemistry of photosynthesis and the gas exchange of leaves. *Planta* **153**: 376–387.

Caldararu S, Thum T, Yu L, Zaehle S. 2020. Whole-plant optimality predicts changes in leaf nitrogen under variable CO_2 and nutrient availability. *New Phytologist* **225**: 2331–2346.

Cannell M. 2000. Modelling the components of plant respiration: some guiding principles. *Annals of Botany* **85**: 45–54.

Chen X, Ciais P, Maignan F, Zhang Y, Bastos A, Liu L, Bacour C, Fan L, Gentine P, Goll D *et al.* 2021. Vapor pressure deficit and sunlight explain seasonality of leaf phenology and photosynthesis across Amazonian evergreen broadleaved forest. *Global Biogeochemical Cycles* **35**: e2020GB006893.

Chu S, Jacobs DF, Sloan JL, Xue L, Wu D, Zeng S. 2018. Changes in soil properties under Eucalyptus relative to *Pinus massoniana* and natural broadleaved forests in South China. *Journal of Forestry Research* **29**: 1299–1306.

Collatz GJ, Ball JT, Grivet C, Berry JA. 1991. Physiological and environmental regulation of stomatal conductance, photosynthesis and transpiration: a model that includes a laminar boundary layer. *Agricultural and Forest Meteorology* **54**: 107–136.

Cooley SS, Fisher JB, Goldsmith GR. 2022. Convergence in water use efficiency within plant functional types across contrasting climates. *Nature Plants* **8**: 341–345.

Cowan IR, Fraquhar GD. 1977. Stomatal function in relation to leaf metabolism and environment. In: Jennings D, ed. *Integration of activity in the higher plant*. Cambridge, UK: Cambridge University Press, 471–505.

Davidson KJ, Lamour J, McPherran A, Rogers A, Serbin SP. 2023. Seasonal trends in leaf-level physiological parameters, obtained through gas exchange, reflectance spectroscopy and, functional trait analysis v.1. *Environmental Data Initiative*. doi: 10.6073/pasta/400eae2df484707ced77d2c2563e3c6c.

Davidson KJ, Lamour J, Serbin SP, Rogers A. 2022. Late day measurement of excised branches results in uncertainty in the estimation of two stomatal parameters derived from response curves in *Populus* 3 deltoides Bartr. × *Populus nigra* L. *Tree Physiology* **42**: 1377–1395.

De Kauwe MG, Kala J, Lin Y-S, Pitman AJ, Medlyn BE, Duursma RA, Abramowitz G, Wang Y-P, Miralles DG. 2015. A test of an optimal stomatal conductance scheme within the CABLE land surface model. *Geoscientific Model Development* **8**: 431–452.

De Kauwe MG, Lin Y-S, Wright IJ, Medlyn BE, Crous KY, Ellsworth DS, Maire V, Prentice IC, Atkin OK, Rogers A *et al.* 2016. A test of the 'one-point method' for estimating maximum carboxylation capacity from field-measured, light-saturated photosynthesis. *New Phytologist* **210**: 1130–1144.

De Kauwe MG, Medlyn BE, Zaehle S, Walker AP, Dietze MC, Hickler T, Jain AK, Luo Y, Parton WJ, Prentice IC *et al.* 2013. Forest water use and water use efficiency at elevated CO_2: a model-data intercomparison at two contrasting temperate forest FACE sites. *Global Change Biology* **19**: 1759–1779.

Dietze MC, Serbin SP, Davidson C, Desai AR, Feng X, Kelly R, Kooper R, LeBauer D, Mantooth J, McHenry K *et al.* 2014. A quantitative assessment of a terrestrial biosphere model's data needs across North American biomes: PEcAn/ED model-data uncertainty analysis. *Journal of Geophysical Research: Biogeosciences* **119**: 286–300.

Drake JE, Power SA, Duursma RA, Medlyn BE, Aspinwall MJ, Choat B, Creek D, Eamus D, Maier C, Pfautsch S *et al.* 2017. Stomatal and non-stomatal limitations of photosynthesis for four tree species under drought: a comparison of model formulations. *Agricultural and Forest Meteorology* **247**: 454–466.

Dreyer E, Le Roux X, Montpied P, Daudet FA, Masson F. 2001. Temperature response of leaf photosynthetic capacity in seedlings from seven temperate tree species. *Tree Physiology* **21**: 223–232.

Duursma RA, Blackman CJ, Lopéz R, Martin-StPaul NK, Cochard H, Medlyn BE. 2019. On the minimum leaf conductance: its role in models of plant water use, and ecological and environmental controls. *New Phytologist* **221**: 693–705.

Ellsworth DS, Reich PB. 1993. Canopy structure and vertical patterns of photosynthesis and related leaf traits in a deciduous forest. *Oecologia* **96**: 169–178.

© 2023 The Authors.
New Phytologist © 2023 New Phytologist Foundation
This article has been contributed to by U.S. Government employees and their work is in the public domain in the USA.

Evans JR, Clarke VC. 2019. The nitrogen cost of photosynthesis. *Journal of Experimental Botany* **70**: 7–15.

Falxa-Raymond N, Patterson AE, Schuster WSF, Griffin KL. 2012. Oak loss increases foliar nitrogen, ^{15}N and growth rates of *Betula lenta* in a northern temperate deciduous forest. *Tree Physiology* **32**: 1092–1101.

Farquhar GD, Sharkey TD. 1982. Stomatal conductance and photosynthesis. *Annual Review of Plant Physiology* **33**: 317–345.

Farquhar GD, von Caemmerer S, Berry JA. 1980. A biochemical model of photosynthetic CO_2 assimilation in leaves of C3 species. *Planta* **149**: 78–90.

Franks PJ, Beerling DJ. 2009. Maximum leaf conductance driven by CO_2 effects on stomatal size and density over geologic time. *Proceedings of the National Academy of Sciences, USA* **106**: 10343–10347.

Franks PJ, Drake PL, Beerling DJ. 2009. Plasticity in maximum stomatal conductance constrained by negative correlation between stomatal size and density: an analysis using *Eucalyptus globulus*. *Plant, Cell & Environment* **32**: 1737–1748.

Gee GW, Federer CA. 1972. Stomatal resistance during senescence of hardwood leaves. *Water Resources Research* **8**: 1456–1460.

Gimeno TE, Saavedra N, Ogée J, Medlyn BE, Wingate L. 2019. A novel optimization approach incorporating non-stomatal limitations predicts stomatal behaviour in species from six plant functional types. *Journal of Experimental Botany* **70**: 1639–1651.

Gourlez de la Motte L, Beauclaire Q, Heinesch B, Cuntz M, Foltýnová L, Šigut L, Kowalska N, Manca G, Ballarin IG, Vincke C *et al.* 2020. Non-stomatal processes reduce gross primary productivity in temperate forest ecosystems during severe edaphic drought. *Philosophical Transactions of the Royal Society of London. Series B: Biological Sciences* **375**: 20190527.

Granda E, Baumgarten F, Gessler A, Gil-Pelegrin E, Peguero-Pina JJ, Sancho-Knapik D, Zimmermann NE, Resco de Dios V. 2020. Day length regulates seasonal patterns of stomatal conductance in *Quercus* species. *Plant, Cell & Environment* **43**: 28–39.

Grassi G, Magnani F. 2005. Stomatal, mesophyll conductance and biochemical limitations to photosynthesis as affected by drought and leaf ontogeny in ash and oak trees. *Plant, Cell & Environment* **28**: 834–849.

Grassi G, Vicinelli E, Ponti F, Cantoni L, Magnani F. 2005. Seasonal and interannual variability of photosynthetic capacity in relation to leaf nitrogen in a deciduous forest plantation in northern Italy. *Tree Physiology* **25**: 349–360.

Héroult A, Lin Y-S, Bourne A, Medlyn BE, Ellsworth DS. 2013. Optimal stomatal conductance in relation to photosynthesis in climatically contrasting *Eucalyptus* species under drought: stomatal responses of eucalyptus under drought. *Plant, Cell & Environment* **36**: 262–274.

Hikosaka K, Nabeshima E, Hiura T. 2007. Seasonal changes in the temperature response of photosynthesis in canopy leaves of *Quercus crispula* in a cool-temperate forest. *Tree Physiology* **27**: 1035–1041.

Jefferson JL, Maxwell RM, Constantine PG. 2017. Exploring the sensitivity of photosynthesis and stomatal resistance parameters in a land surface model. *Journal of Hydrometeorology* **18**: 879–915.

Jiang C, Ryu Y, Wang H, Keenan TF. 2020. An optimality-based model explains seasonal variation in C3 plant photosynthetic capacity. *Global Change Biology* **26**: 6493–6510.

Jin J, Yan T, Wang H, Ma X, He M, Wang Y, Wang W, Guo F, Cai Y, Zhu Q *et al.* 2022. Improved modeling of canopy transpiration for temperate forests by incorporating a LAI-based dynamic parametrization scheme of stomatal slope. *Agricultural and Forest Meteorology* **326**: 109157.

Jin J, Zhan W, Wang Y, Gu B, Wang W, Jiang H, Lu X, Zhang X. 2017. Water use efficiency in response to interannual variations in flux-based photosynthetic onset in temperate deciduous broadleaf forests. *Ecological Indicators* **79**: 122–127.

Kane CN, Jordan GJ, Jansen S, McAdam SAM. 2020. A permeable cuticle, not open stomata, is the primary source of water loss from expanding leaves. *Frontiers in Plant Science* **11**: 774.

Kattge J, Díaz S, Lavorel S, Prentice IC, Leadley P, Bönisch G, Garnier E, Westoby M, Reich PB, Wright IJ *et al.* 2011. TRY – a global database of plant traits. *Global Change Biology* **17**: 2905–2935.

Kattge J, Knorr W, Raddatz T, Wirth C. 2009. Quantifying photosynthetic capacity and its relationship to leaf nitrogen content for global-scale terrestrial biosphere models. *Global Change Biology* **16**: 976–991.

Krinner G, Viovy N, de Noblet-Ducoudré N, Ogée J, Polcher J, Friedlingstein P, Ciais P, Sitch S, Prentice IC. 2005. A dynamic global vegetation model for studies of the coupled atmosphere–biosphere system: DVGM for coupled climate studies. *Global Biogeochemical Cycles* **19**: 2003GB002199.

Lamour J, Davidson KJ, Ely KS, Le Moguédec G, Anderson JA, Li Q, Calderón O, Koven CD, Wright SJ, Walker AP *et al.* 2023. The effect of the vertical gradients of photosynthetic parameters on the CO_2 assimilation and transpiration of a Panamanian tropical forest. *New Phytologist* **238**: 2345–2362.

Lamour J, Serbin SP. 2021. LeafGasExchange. *Zenodo*. doi: 10.5281/zenodo.4545818.

Leakey ADB, Bernacchi CJ, Ort DR, Long SP. 2006. Long-term growth of soybean at elevated [CO_2] does not cause acclimation of stomatal conductance under fully open-air conditions. *Plant, Cell & Environment* **29**: 1794–1800.

Leuning R. 2002. Temperature dependence of two parameters in a photosynthesis model: temperature dependence of photosynthetic parameters. *Plant, Cell & Environment* **25**: 1205–1210.

Li Q, Serbin SP, Lamour J, Davidson KJ, Ely KS, Rogers A. 2022. Implementation and evaluation of the unified stomatal optimization approach in the Functionally Assembled Terrestrial Ecosystem Simulator (FATES). *Geoscientific Model Development* **15**: 4313–4329.

Lin Y-S, Medlyn BE, Duursma RA, Prentice IC, Wang H, Baig S, Eamus D, de Dios VR, Mitchell P, Ellsworth DS *et al.* 2015. Optimal stomatal behaviour around the world. *Nature Climate Change* **5**: 459–464.

Long SP, Bernacchi CJ. 2003. Gas exchange measurements, what can they tell us about the underlying limitations to photosynthesis? Procedures and sources of error. *Journal of Experimental Botany* **54**: 2393–2401.

Long SP, Hällgren J-E. 1993. Measurement of CO_2 assimilation by plants in the field and the laboratory. In: Hall DO, Scurlock JMO, Bolhàr-Nordenkampf HR, Leegood RC, Long SP, eds. *Photosynthesis and production in a changing environment: a field and laboratory manual*. Dordrecht, the Netherlands: Springer Netherlands, 129–167.

Luo X, Keenan TF, Chen JM, Croft H, Colin Prentice I, Smith NG, Walker AP, Wang H, Wang R, Xu C *et al.* 2021. Global variation in the fraction of leaf nitrogen allocated to photosynthesis. *Nature Communications* **12**: 4866.

Machado R, Loram-Lourenço L, Farnese FS, Alves RDFB, Sousa LF, Silva FG, Filho SCV, Torres-Ruiz JM, Cochard H, Menezes-Silva PE. 2021. Where do leaf water leaks come from? Trade-offs underlying the variability in minimum conductance across tropical savanna species with contrasting growth strategies. *New Phytologist* **229**: 1415–1430.

Márquez DA, Stuart-Williams H, Farquhar GD. 2021. An improved theory for calculating leaf gas exchange more precisely accounting for small fluxes. *Nature Plants* **7**: 317–326.

Márquez DA, Stuart-Williams H, Farquhar GD, Busch FA. 2022. Cuticular conductance of adaxial and abaxial leaf surfaces and its relation to minimum leaf surface conductance. *New Phytologist* **233**: 156–168.

Martínez-Vilalta J, Garcia-Forner N. 2017. Water potential regulation, stomatal behaviour and hydraulic transport under drought: deconstructing the iso/anisohydric concept: deconstructing the iso/anisohydric concept. *Plant, Cell & Environment* **40**: 962–976.

McDowell NG, Adams HD, Bailey JD, Hess M, Kolb TE. 2006. Homeostatic maintenance of ponderosa pine gas exchange in response to stand density changes. *Ecological Applications* **16**: 1164–1182.

Medlyn BE, Badeck F-W, De Pury DGG, Barton CVM, Broadmeadow M, Ceulemans R, De Angelis P, Forstreuter M, Jach ME, Kellomäki S *et al.* 1999. Effects of elevated [CO_2] on photosynthesis in European forest species: a meta-analysis of model parameters: photosynthetic acclimation to elevated CO_2. *Plant, Cell & Environment* **22**: 1475–1495.

Medlyn BE, Duursma RA, Eamus D, Ellsworth DS, Prentice IC, Barton CVM, Crous KY, De Angelis P, Freeman M, Wingate L. 2011. Reconciling the optimal and empirical approaches to modelling stomatal conductance. *Global Change Biology* **17**: 2134–2144.

Medvigy D, Jeong S-J, Clark KL, Skowronski NS, Schäfer KVR. 2013. Effects of seasonal variation of photosynthetic capacity on the carbon fluxes of a temperate deciduous forest: seasonality of photosynthetic capacity. *Journal of Geophysical Research: Biogeosciences* **118**: 1703–1714.

Medvigy D, Wofsy SC, Munger JW, Hollinger DY, Moorcroft PR. 2009. Mechanistic scaling of ecosystem function and dynamics in space and time:

© 2023 The Authors.
New Phytologist © 2023 New Phytologist Foundation
This article has been contributed to by U.S. Government employees and their work is in the public domain in the USA.

14698137, 2023, 1, Downloaded from https://nph.onlinelibrary.wiley.com/doi/10.1111/nph.19137 by Columbia University Libraries, Wiley Online Library on [05/09/2024]. See the Terms and Conditions (https://onlinelibrary.wiley.com/terms-and-conditions) on Wiley Online Library for rules of use; OA articles are governed by the applicable Creative Commons License

ecosystem demography model v.2. *Journal of Geophysical Research* **114**: G01002.

Meir P, Kruijt B, Broadmeadow M, Barbosa E, Kull O, Carswell F, Nobre A, Jarvis PG. 2002. Acclimation of photosynthetic capacity to irradiance in tree canopies in relation to leaf nitrogen concentration and leaf mass per unit area: photosynthetic acclimation in forest canopies. *Plant, Cell & Environment* **25**: 343–357.

Mengoli G, Agustí-Panareda A, Boussetta S, Harrison SP, Trotta C, Prentice IC. 2022. Ecosystem photosynthesis in land-surface models: a first-principles approach incorporating acclimation. *Journal of Advances in Modeling Earth Systems* **14**: e2021MS002767.

Miao Y, Cai Y, Wu H, Wang D. 2021. Diurnal and seasonal variations in the photosynthetic characteristics and the gas exchange simulations of two rice cultivars grown at ambient and elevated CO_2. *Frontiers in Plant Science* **12**: 651606.

Misson L, Tu KP, Boniello RA, Goldstein AH. 2006. Seasonality of photosynthetic parameters in a multi-specific and vertically complex forest ecosystem in the Sierra Nevada of California. *Tree Physiology* **26**: 729–741.

Muir CD. 2019. TEALEAVES: an R package for modelling leaf temperature using energy budgets. *AoB PLANTS* **11**: plz054.

Muñoz Sabater J. 2019. ERA5-land hourly data from 1950 to present. Copernicus Climate Change Service (C3S) Climate Data Store (CDS). doi: 10.24381/cds.e2161bac.

Norman JM. 1979. Modeling the complete crop canopy. In: Barfield G, ed. *Modification of the aerial environment of crops*. St Joseph, MI, USA: American Society of Agricultural Engineers, 249–277.

O'Leary BM, Asao S, Millar AH, Atkin OK. 2019. Core principles which explain variation in respiration across biological scales. *New Phytologist* **222**: 670–686.

Oleson KW, Lawrence DM, Bonan GB, Drewniak B, Huang M, Levis S, Li F, Riley WJ, Swenson SC, Thornton PE *et al.* 2013. *Technical description of v.4.5 of the Community Land Model (CLM).* Boulder, CO, USA: National Center for Atmospheric Research.

Ow LF, Whitehead D, Walcroft AS, Turnbull MH. 2010. Seasonal variation in foliar carbon exchange in *Pinus radiata* and *Populus deltoides*: respiration acclimates fully to changes in temperature but photosynthesis does not: acclimation of respiration but not photosynthesis in trees. *Global Change Biology* **16**: 288–302.

Pantin F, Simonneau T, Muller B. 2012. Coming of leaf age: control of growth by hydraulics and metabolics during leaf ontogeny. *New Phytologist* **196**: 349–366.

Pinheiro J, Bates D, DebRoy S, Sarkar D, Heisterkamp S, Bert VW. 2020. *Package 'NLME'.*

Prikaziuk E, Migliavacca M, Su Z(B), van der Tol C. 2023. Simulation of ecosystem fluxes with the SCOPE model: sensitivity to parametrization and evaluation with flux tower observations. *Remote Sensing of Environment* **284**: 113324.

Quebbeman JA, Ramirez JA. 2016. Optimal allocation of leaf-level nitrogen: implications for covariation of V_{cmax} and J_{max} and photosynthetic downregulation: covariation of V_{cmax} and J_{max}. *Journal of Geophysical Research: Biogeosciences* **121**: 2464–2475.

R Core Team. 2013. *R: a language and environment for statistical computing.* Vienna, Austria: R Foundation for Statistical Computing.

Raesch A. 2020. *PVLDCURVE: simplifies the analysis of pressure volume and leaf drying curves.* [WWW document] URL https://cran.r-project.org/web/packages/pvldcurve/index.html [accessed 16 May 2021].

Reich PB. 2014. The world-wide 'fast–slow' plant economics spectrum: a traits manifesto. *Journal of Ecology* **27**: 275–301.

Reich PB, Wright IJ, Lusk CH. 2007. Predicting leaf physiology from simple plant and climate attributes: a global GLOPNET analysis. *Ecological Applications* **17**: 1982–1988.

Ricciuto D, Sargsyan K, Thornton P. 2018. The impact of parametric uncertainties on biogeochemistry in the E3SM land model. *Journal of Advances in Modeling Earth Systems* **10**: 297–319.

Rodriguez-Dominguez CM, Forner A, Martorell S, Choat B, Lopez R, Peters JMR, Pfautsch S, Mayr S, Carins-Murphy MR, McAdam SAM *et al.* 2022. Leaf water potential measurements using the pressure chamber: synthetic testing of assumptions towards best practices for precision and accuracy. *Plant, Cell & Environment* **45**: 2037–2061.

Rogers A. 2014. The use and misuse of $V_{c,max}$ in Earth system models. *Photosynthesis Research* **119**: 15–29.

Rogers A, Medlyn BE, Dukes JS, Bonan G, von Caemmerer S, Dietze MC, Kattge J, Leakey ADB, Mercado LM, Niinemets Ü *et al.* 2017. A roadmap for improving the representation of photosynthesis in Earth system models. *New Phytologist* **213**: 22–42.

Sabot MEB, Kauwe MG, Pitman AJ, Medlyn BE, Ellsworth DS, Martin-StPaul N, Wu J, Choat B, Limousin J, Mitchell PJ *et al.* 2022. One stomatal model to rule them all? Towards improved representation of carbon and water exchange in global models. *Journal of Advances in Modeling Earth Systems* **14**: e2021MS002761.

Sala A, Tenhunen JD. 1996. Simulations of canopy net photosynthesis and transpiration in *Quercus ilex* L. under the influence of seasonal drought. *Agricultural and Forest Meteorology* **78**: 203–222.

Sanchez A, Hughes N, Smith W. 2013. Water-use efficiency declines during autumn leaf senescence in three deciduous tree species. *International Journal of Plant Biology* **4**: e7.

Sang Y, Wang C, Huo H. 2011. Inter-specific and seasonal variations in photosynthetic capacity and water use efficiency of five temperate tree species in Northeastern China. *Scandinavian Journal of Forest Research* **26**: 21–29.

Scholander PF, Hammel HT, Hemmingsen EA, Bradstreet ED. 1964. Hydrostatic pressure and osmotic potential in leaves of mangroves and some other plants. *Proceedings of the National Academy of Sciences, USA* **52**: 119–125.

Schuster WSF, Griffin KL, Roth H, Turnbull MH, Whitehead D, Tissue DT. 2008. Changes in composition, structure and aboveground biomass over seventy-six years (1930–2006) in the Black Rock Forest, Hudson Highlands, southeastern New York State. *Tree Physiology* **28**: 537–549.

Serbin SP, Singh A, McNeil BE, Kingdon CC, Townsend PA. 2014. Spectroscopic determination of leaf morphological and biochemical traits for northern temperate and boreal tree species. *Ecological Applications* **24**: 1651–1669.

Slot M, Winter K. 2017. *In situ* temperature relationships of biochemical and stomatal controls of photosynthesis in four lowland tropical tree species. *Plant, Cell & Environment* **40**: 3055–3068.

Smith NG, Keenan TF, Colin Prentice I, Wang H, Wright IJ, Niinemets Ü, Crous KY, Domingues TF, Guerrieri R, Yoko Ishida F *et al.* 2019. Global photosynthetic capacity is optimized to the environment. *Ecology Letters* **22**: 506–517.

Sperlich D, Barbeta A, Ogaya R, Sabaté S, Peñuelas J. 2016. Balance between carbon gain and loss under long-term drought: impacts on foliar respiration and photosynthesis in *Quercus ilex* L. *Journal of Experimental Botany* **67**: 821–833.

Sperry JS. 2013. Cutting-edge research or cutting-edge artefact? An overdue control experiment complicates the xylem refilling story: xylem-refilling artefacts. *Plant, Cell & Environment* **36**: 1916–1918.

Stokes VJ, Morecroft MD, Morison JIL. 2010. Comparison of leaf water use efficiency of oak and sycamore in the canopy over two growing seasons. *Trees* **24**: 297–306.

Turnbull MH, Whitehead D, Tissue DT, Schuster WSF, Brown KJ, Griffin KL. 2001. Responses of leaf respiration to temperature and leaf characteristics in three deciduous tree species vary with site water availability. *Tree Physiology* **21**: 571–578.

Von Caemmerer S. 2013. Steady-state models of photosynthesis: steady-state models of photosynthesis. *Plant, Cell & Environment* **36**: 1617–1630.

Wang H, Atkin OK, Keenan TF, Smith NG, Wright IJ, Bloomfield KJ, Kattge J, Reich PB, Prentice IC. 2020. Acclimation of leaf respiration consistent with optimal photosynthetic capacity. *Global Change Biology* **26**: 2573–2583.

Wang Q, Iio A, Tenhunen J, Kakubari Y. 2008. Annual and seasonal variations in photosynthetic capacity of *Fagus crenata* along an elevation gradient in the Naeba Mountains, Japan. *Tree Physiology* **28**: 277–285.

Wang Q, Tenhunen J, Falge E, Bernhofer C, Granier A, Vesala T. 2004. Simulation and scaling of temporal variation in gross primary production for coniferous and deciduous temperate forests: physiological effects on temperate forest. *Global Change Biology* **10**: 37–51.

Wang X, Chen JM, Ju W, Zhang Y. 2022. Seasonal variations in leaf maximum photosynthetic capacity and its dependence on climate factors across global

© 2023 The Authors.
New Phytologist © 2023 New Phytologist Foundation
This article has been contributed to by U.S. Government employees and their work is in the public domain in the USA.

14698137, 2023, 1, Downloaded from https://nph.onlinelibrary.wiley.com/doi/10.1111/nph.19137 by Columbia University Libraries, Wiley Online Library on [05/09/2024]. See the Terms and Conditions (https://onlinelibrary.wiley.com/terms-and-conditions) on Wiley Online Library for rules of use; OA articles are governed by the applicable Creative Commons License

FLUXNET sites. *Journal of Geophysical Research: Biogeosciences* **127**: e2021JG006709.

Wardle K, Short KC. 1983. Stomatal responses and the senescence of leaves. *Annals of Botany* **52**: 411–412.

Way DA, Montgomery RA. 2015. Photoperiod constraints on tree phenology, performance and migration in a warming world. *Plant, Cell & Environment* **38**: 1725–1736.

Wehr R, Munger JW, McManus JB, Nelson DD, Zahniser MS, Davidson EA, Wofsy SC, Saleska SR. 2016. Seasonality of temperate forest photosynthesis and daytime respiration. *Nature* **534**: 680–683.

Wilson KB, Baldocchi DD, Hanson PJ. 2000a. Spatial and seasonal variability of photosynthetic parameters and their relationship to leaf nitrogen in a deciduous forest. *Tree Physiology* **20**: 565–578.

Wilson KB, Baldocchi DD, Hanson PJ. 2000b. Quantifying stomatal and non-stomatal limitations to carbon assimilation resulting from leaf aging and drought in mature deciduous tree species. *Tree Physiology* **20**: 787–797.

Wilson KB, Baldocchi DD, Hanson PJ. 2001. Leaf age affects the seasonal pattern of photosynthetic capacity and net ecosystem exchange of carbon in a deciduous forest: leaf age and net ecosystem exchange of carbon. *Plant, Cell & Environment* **24**: 571–583.

Wong SC, Cowan IR, Farquhar GD. 1979. Stomatal conductance correlates with photosynthetic capacity. *Nature* **282**: 424–426.

Wong SC, Cowan IR, Farquhar GD. 1985. Leaf conductance in relation to rate of CO_2 assimilation. *Plant Physiology* **78**: 821–825.

Wright IJ, Leishman MR, Read C, Westoby M. 2006. Gradients of light availability and leaf traits with leaf age and canopy position in 28 Australian shrubs and trees. *Functional Plant Biology* **33**: 407–419.

Wright IJ, Reich PB, Westoby M, Ackerly DD, Baruch Z, Bongers F, Cavender-Bares J, Chapin T, Cornelissen JHC, Diemer M *et al.* 2004. The worldwide leaf economics spectrum. *Nature* **428**: 821–827.

Xie J, Zha T, Zhou C, Jia X, Yu H, Yang B, Chen J, Zhang F, Wang B, Bourque CP-A *et al.* 2016. Seasonal variation in ecosystem water use efficiency in an urban-forest reserve affected by periodic drought. *Agricultural and Forest Meteorology* **221**: 142–151.

Xu L, Baldocchi DD. 2003. Seasonal trends in photosynthetic parameters and stomatal conductance of blue oak (*Quercus douglasii*) under prolonged summer drought and high temperature. *Tree Physiology* **23**: 865–877.

Yang D, Meng R, Morrison BD, McMahon A, Hantson W, Hayes DJ, Breen AL, Salmon VG, Serbin SP. 2020. A multi-sensor unoccupied aerial system improves characterization of vegetation composition and canopy properties in the arctic tundra. *Remote Sensing* **12**: 2638.

Yang X, Tang J, Mustard JF, Wu J, Zhao K, Serbin S, Lee J-E. 2016. Seasonal variability of multiple leaf traits captured by leaf spectroscopy at two temperate deciduous forests. *Remote Sensing of Environment* **179**: 1–12.

Zhou S-X, Medlyn B, Sabaté S, Sperlich D, Prentice IC, Whitehead D. 2014. Short-term water stress impacts on stomatal, mesophyll and biochemical limitations to photosynthesis differ consistently among tree species from contrasting climates. *Tree Physiology* **34**: 1035–1046.

Zhu G-F, Li X, Su Y-H, Lu L, Huang C-L. 2011. Seasonal fluctuations and temperature dependence in photosynthetic parameters and stomatal conductance at the leaf scale of *Populus euphratica* Oliv. *Tree Physiology* **31**: 178–195.

Supporting Information

Additional Supporting Information may be found online in the Supporting Information section at the end of the article.

Fig. S1 Evaluation of individual residuals for the maple and white oak species groups.

Fig. S2 Average monthly estimates of leaf mass per area (LMA), leaf dry matter content (LDMC), elemental nitrogen per unit mass (N_{mass}), elemental nitrogen per unit area (N_{area}), ratio of foliar carbon to nitrogen (C : N), stomatal density, and the ratio between the dark respiration rate normalized to 25°C ($R_{dark.25}$) and the maximum carboxylation capacity of Rubisco normalized to 25°C ($V_{cmax.25}$) by species group for the 2021 growth season.

Fig. S3 Frequency distributions of the level of the relative strength of the stomatal limitation on photosynthesis (I, where $I = 0$ represents no stomatal limitation on photosynthesis while a value of $I = 1$ represents complete stomatal limitation on photosynthesis).

Fig. S4 Relationships between leaf-to-air VPD, PAR, and air temperature, and the level of stomatal limitation on photosynthesis (I, where $I = 0$ represents no stomatal limitation on photosynthesis while a value of $I = 1$ represents complete stomatal limitation on photosynthesis) for all observations where $I > 0$.

Fig. S5 Average monthly relative water deficit at turgor loss and predawn Ψ_{leaf} by species group for the 2021 growth season.

Table S1 Group-specific parameters used in the coupled photosynthesis, conductance, and energy balance models used for simulations in this study.

Table S2 Values for mean monthly photosynthetic and conductance parameters by species group. Each sample represents an independent leaf-level estimate.

Please note: Wiley is not responsible for the content or functionality of any Supporting Information supplied by the authors. Any queries (other than missing material) should be directed to the *New Phytologist* Central Office.

© 2023 The Authors.
New Phytologist © 2023 New Phytologist Foundation
This article has been contributed to by U.S. Government employees and their work is in the public domain in the USA.

14698137, 2023, 1, Downloaded from https://nph.onlinelibrary.wiley.com/doi/10.1111/nph.19137 by Columbia University Libraries, Wiley Online Library on [05/09/2024]. See the Terms and Conditions (https://onlinelibrary.wiley.com/terms-and-conditions) on Wiley Online Library for rules of use; OA articles are governed by the applicable Creative Commons License